LTH
FACULTY OF ENGINEERING

Department of Biomedical Engineering
in collaboration with
Tetra Pak® Packaging Solutions AB

Developing a Virtual Consumer
-From Human Skin to FE Modelling

Master's Thesis in Biomedical Engineering by

Gustaf Svanberg

and

Viktor Hultgren

Spring 2019

Supervisors:
M. Sc. Eskil Andreasson, Tetra Pak® Packaging Solutions AB
Prof. Hanna Isaksson, Dep. of Biomedical Engineering

Examiner:
Ph. D. Lorenzo Grassi, Dep. of Biomedical Engineering

Abstract

In the 'on-the-go' society of today, the use of single unit beverage packages has increased. Consequently, the interaction between the consumer and the package have also attracted greater interest when trying to gain advantages in a competitive market. One way of gaining such an advantage is by decreasing the developing costs of products: either by reducing time spent, or money invested in prototypes. Virtual testing provides a solution to both these scenarios and is something which Tetra Pak® in particular, has become interested in. Using two different package opening devices in an initial trial for virtual testing, this work set out to evaluate the prospect of using simulations as a new tool in evaluating these frames and investigating their interaction with a virtual human-like consumer.

To model this virtual consumer the mechanical properties of human soft tissue, skin (*dermis*) in particular, have been investigated. Using hyperelastic material models a suitable material was formulated using inverse FE modelling and an experimental validation from existing literature. This material model was then used in dynamic 2D and 3D simulations using ABAQUS®, where the interaction between package opening devices and the consumer was studied.

The result consists of two parts: Firstly, a configuration of a Neo-Hookean and a single term Ogden material, which replicates human facial tissue well enough to provide realistic deformation and stress within a $[-0.4, 0.15]$ true strain range. Secondly, a methodology of how package opening devices may be evaluated and how to model a drinking motion to replicate a human drinking action.

Future prospects of this work could be to integrate it in the design process of a number of different opening devices. Enabling pre-production evaluation of designs, which could shorten the developing time needed and also reduce the waste material from failed designs. Moreover, it could also be used as a tool in improving the drinking experience of consumers if for instance strain measures are connected with pleasantness by performing consumer tests.

Keywords: Dermis, Human soft tissue, FEM

Acknowledgements

We would like to acknowledge and thank our supervisors M. Sc. Eskil Andreasson and Prof. Hanna Isaksson. Eskil for his support, guidance and help. His seemingly inexhaustible source of commitment has played a key role through all steps in this thesis. His visionary thinking has not only helped us, but also inspired us and taught us valuable lessons regarding research and development.

Hanna for her profound knowledge within the field of biomechanics, which provided us with the tools to grasp this subject much quicker than would otherwise be possible and also for her tips throughout the work, both practical and during our writing, guiding us onto the right track.

We would also like to express our gratitude towards Viktor Petersson and Bengt Håkansson for participating in weekly meetings, providing insightful discussions which have been of great importance. Viktor deserves an extra thanks for taking his time answering questions and providing support whenever needed.

A special thanks is directed to Johan Nordgren for providing education in using Hypermesh™ giving us a head start, and also for answering questions related to the software.

Last but not least, we would like to thank our friends and families–thank you for all the love and laughter.

Lund, March 2019
Gustaf & Viktor

List of Abbreviations

2D	Two dimensional
3D	Three dimensional
A38	Opening device of the *Tetra Top*® 200ml
AE	Almost Empty
BC	Boundary Condition
DC	*DreamCap*™
ECM	Extra Cellular Matrix
F	Full
FE	Finite Element
FEM	Finite Element Method
GOH	Gasser-Ogden-Holzapfel
IV	Initial Value
LASTIC®	Light Aspiration device for in vivo Soft TIssue Characterisation
MIDA	Multi-modal Imaging based Detailed Anatomical model
MRI	Magnetic Resonance Imaging
N-H	Neo Hookean
PDE	Partial Differential Equation
PPT	Pressure Pain Threshold
PPTO	Pressure Pain Tolerance
STD	Standard Deviation
UTS	Ultimate Tensile Strength

Contents

1 Introduction **3**
1.1 Scientific Aim and/or Scope 5

2 Background **7**
2.1 Human Soft Tissue 7
2.2 Mechanical Properties of Skin 11
2.3 Constitutive Equations 14
2.3.1 Material Models 15

3 Human Skin Modelling **19**
3.1 Method 20
3.1.1 Material Model Analysis 20
3.1.2 Material Model Calibration 22
3.1.3 Material Model Validation 26
3.2 Results and Analysis 27
3.2.1 Material Model Analysis 27
3.2.2 Material Model Calibration 30
3.2.3 Material Model Validation 37

4 Drinking Sequence Modelling **43**
4.1 Method 44
4.1.1 Drink Sequence Motion Capture 44
4.1.2 Drink Sequence Simulation 45
4.2 Results and Analysis 52
4.2.1 Motion Capture and the 2D Virtual Head Cross Section 52
4.2.2 3D Partitioned Virtual Head 61

5 Discussion **73**
5.1 Future work 74

6 Conclusion **77**

Appendix A Complementing Theory **83**

Chapter 1

Introduction

Engineers generally work with quantitative entities, thus when being faced with a proposal for a thesis work involving 'drinking experience' the first thought was: how can this be measured? Evidently one must first define optimal in context to some criteria. Furthermore the criteria chosen must be interpreted similarly among the test subjects, people in general are dissimilar and one cannot list all the reasons why a person might like or dislike a product placed in front of them: In Tetra Pak®'s case: Do the consumers like the colour of a certain package design? Will this opinion affect the thoughts on the size of the design? Was it the taste of the product that made them disapprove of the package? These kinds of noises may be suppressed in an easy fashion by not utilising persons at all.

Favourably one would want a model without noise, without feelings, which can answer simply put questions. Questions which in turn will produce an answer to the stated want of an answer to: What is an optimal package design? Such a model could be constructed in a laboratory environment, but then a further improvement on how to ease product development would be to take this physical model and create a digitised version enabling testing without the need of producing any physical designs, hopefully reducing costs and time required for each design. This is the starting point of this thesis: namely to describe means of creating a drinking simulator. With such a simulator Tetra Pak® would be able to test designs of their packages prior to production. This would enable product development to be partly performed in a digital environment.

Computational studies concerning product development are already being performed: For example Grooves *et al.* [18] used a multilayered Finite Element (FE) model to evaluate the design of micro needles designed to penetrate the skin barrier for drug distribution. Or for instance the use of human-like models in the car industry in the development of car seats. The model

can reduce the need for physical testing and thus also decouple the subjective opinions of test persons from the data of the tests [31]. Moreover in a simulator all output is fully available. One is not limited to look at, for instance, surface deformations or contact areas. The state of the material throughout the domain is readily available and more advanced analysis may be performed.

Narrowing down the scope of investigation, special care will be taken to product designs that are encouraging consumption 'on-the-go', i.e. designs produced to be consumed straight out of the package. This type of consumption is getting increasingly popular [36] and several designs have been developed with this in mind, two of which will be investigated in this work: Firstly, the *Tetra Prisma® Aseptic* with the *DreamCap™* opening device, which from here on after will be referred to as the *DC* frame or opening device. Secondly, there is the *Tetra Top®* 200ml and its opening device from here on after being referred to as the *A38* opening device or frame. The packages and their respective opening devices are seen in Figure 1.1.

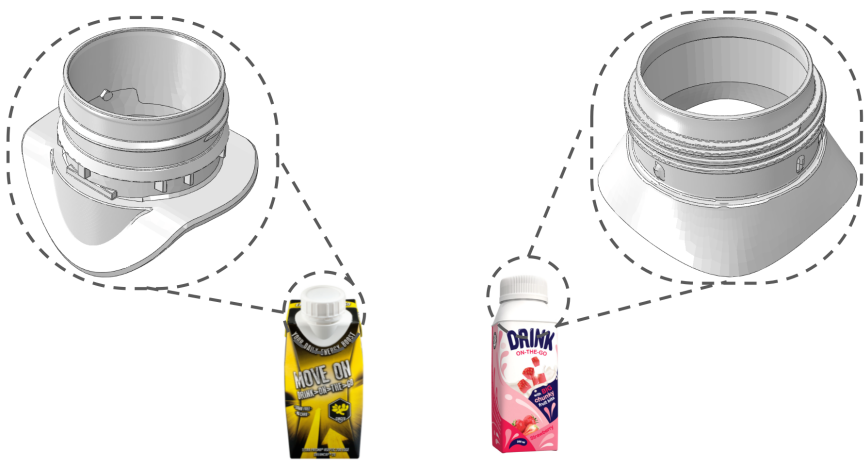

(a) The DC opening device.

(b) The A38 opening device

Figure 1.1: a) *Tetra Prisma® Aseptic* with its DC opening device. b) The *Tetra Top®* 200ml with its A38 opening device.

What about the material present? Is it important with an accurate description of the facial tissue when developing a simulator to perform virtual product evaluation? Take surgery treating cleft-lip as an example [25]. The objective of using simulations is to reduce further need of surgery by predicting the outcome of the initial intervention. Another area of interest is animation in computer games or movies [40], where models have been constructed taking advantage of non-linear finite element simulations to reproduce facial expressions controlled by muscles. When simulating facial tissue, the need for accurate descriptions of the tissue is apparent, as the material choice will

govern the deformation of the face.

Combining the above, our intention is to describe a suitable method to evaluate package designs using FE simulations to find more optimised designs earlier in the design process.

1.1 Scientific Aim and/or Scope

Tetra Pak® is one of many companies starting to look for alternative methods during the design phase of their products. In this thesis we will evaluate the possibilities of using a virtual consumer as a mean of evaluating critical design criteria of package opening devices influencing the drinking experience. This is done by:

1. A literature study to find suitable material models, which accurately describes facial soft tissue.
2. Simulations employing the FEM, in which the found material model is investigated, as well as experimental validation of the material connected to our application of package/consumer interaction.
3. Analysing the interaction and contact between a beverage package and a consumer.

In order to reach these goals, the workflow shown in Figure 1.2 was employed. The thesis begins with the chapter *Background* in which information regarding human skin, the mechanical properties of human skin and how it has previously been modelled is collected. Then the thesis continues into the chapter *Human Skin Modelling* where the gathered information is used to calibrate and validate a material suitable for the application in mind. This material is then used as input into the next chapter, *Drinking Sequence Modelling*. In that chapter, the validated material is used together with motion capture and a fully realistic computer model of a human head producing 2D- and 3D-simulations. The results from both the *Human Skin Modelling* and the *Drinking Sequence Modelling* are then summarised in the *Conclusion*.

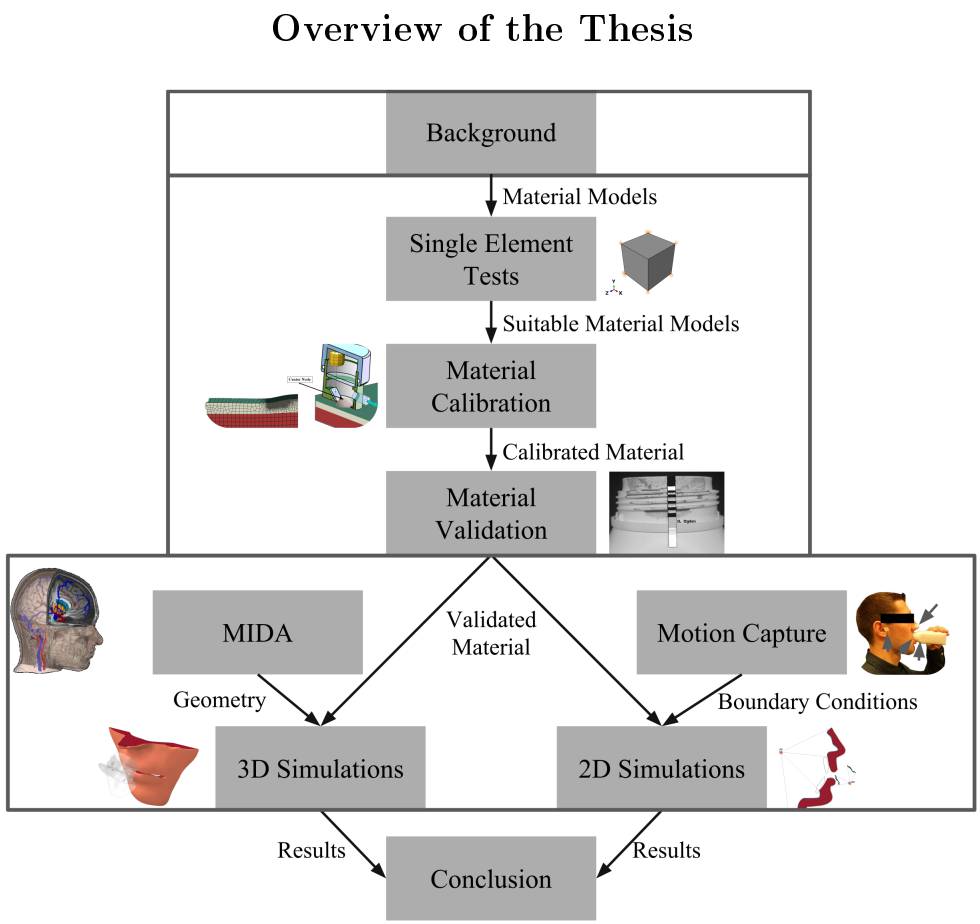

Figure 1.2: The workflow employed in this thesis, where chapters are enclosed by grey borders and sections are represented by grey boxes. The small text next to the arrows are the outputs and inputs for the sections (e.g Calibrated Material is the output from Material Calibration and the input to Material Validation).

Chapter 2

Background

Before modelling human soft tissue, the properties and previous material modelling attempts are investigated. This chapter starts with creating a foundation of what human soft tissue really means, and then progresses onto what defines human skin. Finally the differences between skin depending on: location, person, age and gender are described, and how these are related to its mechanical properties.

The mechanical properties of skin are reviewed by a presentation of previous works concerning human skin and thereafter a selection of material models are presented. Finally the foundations for using FE-simulations to simulate complex events is introduced and especially what the material models manage to describe in the simulations. This is done as a preparation for taking the step into modelling human soft tissue.

2.1 Human Soft Tissue

There are four major types of soft tissue in the human body: connective, nervous, epithelial, and muscle. Example of connective tissue would be adipose tissue (fatty tissue) and dense connective tissue such as tendons and/or ligaments. Muscle tissue is divided into three subgroups being: smooth (walls of the arteries for instance), skeletal and cardiac muscle, which is only present in the heart.

Moreover, parts of the skin belong to the epithelial subgroup [11], which is a group of tissues embedding organs within the body, and also controlling the transport of various substances to and from these organs. Other parts of the skin are categorised as dense connective tissue [8]. If organised in a single layer, one may denote the epithelium to be of simple type, whereas layered structures are called stratified epithelium. The epithelial cells connect to other tissue through a basement membrane which takes the form of a Extra Cellular

Matrix (ECM) of proteins fastening the epithelium to the tissue.

The ECM consists of connective tissue serving as a base structure onto which new cells may connect. Investigating it on the μm scale it is built up by a mix of fibres (collagen fibres and elastin fibres, both being proteins) and other non-fibrous proteins [39]. Some of the non-fibrous proteins present are proteoglycans which are proteins carrying a negative charge. This gives them the ability to attract water molecules and thereby proteoglycans have a key role in governing the water content of soft tissue, and thus also contributes to the non-linear behaviour of the material [8]. The water content of the ECM also provides near incompressible material behaviour to the tissue.

Collagen is present in most tissues in different forms and primarily provides tensile strength to the tissue. It is ordered in a highly hierarchical fashion such that fibres consisting of amino acids jointly form bundles, resembling rope or wire structures, which enhances the tensile strength of the collagen. Most of the collagen present in the body (about 40%) is found in the skin (collagen type III and I) where it forms a heterogeneous web in contrast to collagen in muscoskeletal tissues, e.g. bone, which is more ordered [8].

Elastin's mechanical properties are, in resemblance with collagen, enhanced by the way its fibres are structured. In a dormant, or non load-bearing state, these are wound up and when they are under tension they straighten out. This gives elastin a rubber-like behaviour [8], but still elastin has the most linear-like mechanical behaviour of the biological tissues in the body [16].

To get a sense of the magnititude of the constitutive attributes of biological tissue the elastic modulus and yield stress of a collection of materials are displayed in Table 2.1. Notable is the large range over which the stiffness of the elastin, bone and collagen reaches.

Table 2.1: Material properties of biological tissue with steel as reference. E is referring to the elastic modulus of the material and σ_0 denotes the yield stress. The data is collected from [16].

	E [MPa]	σ_0 [MPa]
Elastin	0.6	-
Collagen (in the fibre direction)	$1 \cdot 10^3$	50-100
Bone (in the osteon direction)	$1 \cdot 10^4$	100
Mild steel	$2 \cdot 10^5$	500

Human skin

The skin is the largest organ of the human body and provides several biological functions, e.g. protection and thermoregulation [18]. Starting from the surface, it is comprised of the *epidermis* and the *dermis*. Beneath the dermis the *hypodermis* is found which mainly consists of adipose tissue, see Figure

Table 2.2: Approximate thickness of the various layers of thick skin. Values are taken from [38].

Layer	Thickness [μm]
Stratum corneum	10-20
Living epidermis	30-130
Dermis	1100
Hypodermis (subcutaneous fat)	1200

2.1. There are two types of skin, thick and thin skin, where the difference being that the thickness of the dermis is thinner for thick skin. Also, thick skin lacks hair follicles, sweat glands and sebaceous glands. Thick skin is found in the soles of the feet, the fingertips and the palms of the hands (i.e areas which are exposed to a high degree of abrasion) [4].

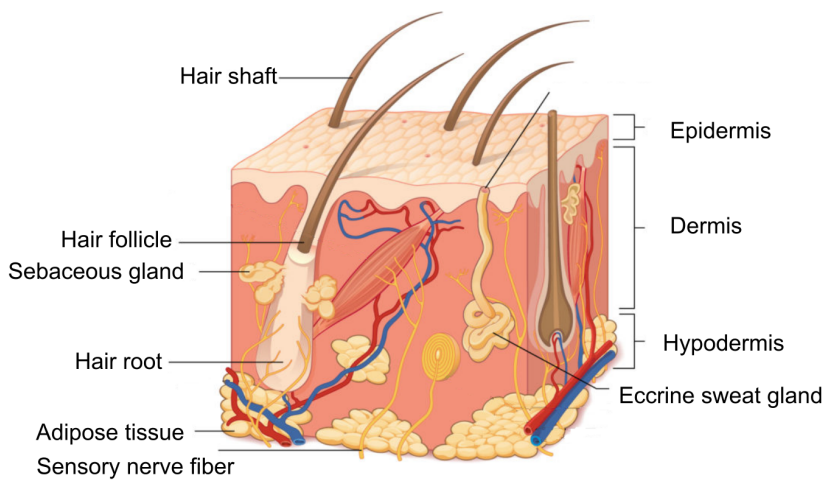

Figure 2.1: The structure of human skin. The figure has been reworked from [7].

The outermost skin layer, the epidermis, consists of several layers of cells that are keratinized to different extent. Roughly, the epidermis can be divided into two layers, the *living epidermis* and the *stratum corneum*. During the course of time, the cells in the epidermis migrate from the innermost layer out towards the surface, forming the stratum corneum at the surface which is comprised of keratin filled dead cells. This process takes about 2-4 weeks [4]. Moreover receptors sensitive to mechanical stimuli are present between the outer layers of the skin. Situated at the epidermal-dermal layers the so called *Merkel cells* are able to detect contact external stimuli [6]. The approximate thickness of the various layers can be found in Table 2.2.

The dermis is the thickest layer of the skin and is primarily made up of type III collagen [28], which make up about 75% of the fat free dry mass (compared

to elastin which makes up about 4%) [24].

The collagen molecules are interlaced, forming collagen fibrils which are aligned in a very heterogeneous fashion in the dermis. One may well imagine this originates from the load bearing function of the skin. Comparing skin to e.g. bone, which has similar fibrils with well defined orientation, the skin must be able to adapt to traction in all directions. Consequently the bone has adapted to more well defined load-paths. Moreover, the tensile behaviour of human dermis is highly influenced by the straightening of the collagen present in the tissue and becomes very stiff when the collagen fibrils are fully elongated and are beginning to stretch (Figure 2.2).

Regarding the differences between regular skin and the lips, the epidermis' outermost layer, the stratum corneum, is much thinner in the lips than in the regular skin. Thus, the skin of the lips is softer than the regular skin, due to the role as a hard protective layer (the outermost 'defence' of the skin) that the stratum corneum plays. Unlike the epidermis in regular skin, the epidermis present in the lips lack melanocytes which are the cells that produces melanin. Melanin is a light absorbing pigment that gives regular skin its color, the more melanin the darker the skin. The combination of no melanin and a thin stratum corneum makes the blood cells in the dermis visible from the outside making the lips appear red [22].

Furthermore, the lips lacks hair follicles, sweat glands and also sebaceous glands. The sebaceous glands provides moisture for the skin and the lack of them in the lips is the reason why lips easily become chapped in dry and or cold climate.

Moreover, the anisotropic nature of skin may be expressed using the concept of Langer's lines. First formulated by A. K. Langer these are paths in the skin along which the tension is highest [24]. Langer noticed that when he punc-

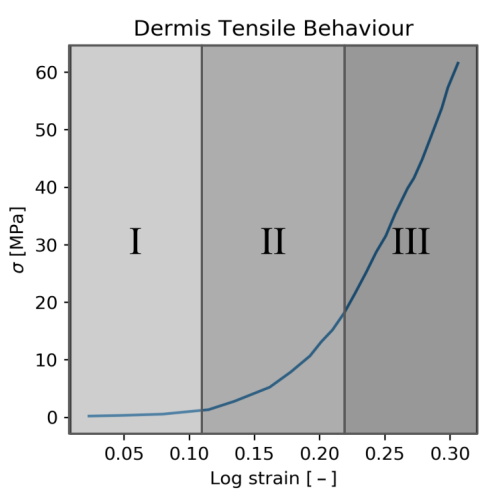

Figure 2.2: The three distinct phases of the dermis where in I) the collagen is starting to straighten, in II) begins to stiffen as more fibres become fully elongated, and lastly in III) is straightened out and very stiff. Data gathered from [32]

tured skin using a circular-tipped tool the wounds he inflicted were elliptical, thus indicating the skin to be anisotropic and pre-stretched.

Lastly, dermal thickness across the facial region has been examined by measuring its thickness at 15 facial sites. Findings were that the relative thicknesses between the upper eyelids and the examined facial sites were consistent between the subjects that were examined. The mean dermal thickness for the upper eyelids was 0.38 ± 0.09 mm and the calculated ratio between the upper eyelids and the chin was 3.14 ± 0.46 [19].

2.2 Mechanical Properties of Skin

In vivo denotes experiments performed on an entity still remaining in its natural, living, surroundings. Such as skin still remaining on the body. Its counterpart would be *ex vivo* meaning that an entity is taken out of its natural surrounding. *In vitro* can be read similar as to *ex vivo* as the entity in question is investigated outside its natural environment, e.g. a laboratory.

There have been several studies trying to determine a suitable material model and corresponding material parameters for *in vivo* skin as a homogeneous material and also some studies trying to do the same for the different layers of skin.

Using indentation tests Bader *et al.* [5] showed that the mechanical response of skin is different depending on the site of the body that is examined, and intra-subject variation. Luboz *et al.* [27] performed *in vivo* suction tests at four different areas in the face and came to the conclusion that the stiffness is dependent on the underlying muscles, the amount of fat and the tissue thickness. Moreover several studies have shown that inter-subject variation of soft tissue properties between test subjects is significant ([27],[3], [15]).

Tran *et al.* [38] used MRI to measure the *in vivo* deformation of the different layers of tissue on a subjects forearm by taking 2D images of a cross-section. By sectioning the tissue into the different layers, creating contours on the 2D image, the deformation of the arm was obtained by minimising the error between the displacement of the outlines of the layers and the FE mesh when the indentation of up to 8 mm depth was simulated. Through this procedure, Neo-Hookean material parameters for the: epidermis, the dermis, the hypodermis and the muscle tissue were obtained.

Nì Annaídh *et al.* [3] performed *ex vivo* tensile testing of human skin (solely dermis) excised from the back of cadavers of several subjects to determine the Ultimate Tensile Strength (UTS) of the dermis (Table 2.3). The same authors also showed that there was a positive correlation between the direction of the Langer's lines of the skin and collagen orientation [32].

Aldieri *et al.* [2] performed validation of material models. Using an inverse

Table 2.3: Values of the UTS (nominal stress) and the failure strain (engineering strain) of human dermis gathered from literature.

Paper	UTS [MPa]	Failure strain [%]	Bodysite
Jensen & Rottier [26]	1-24	17-207	Abdomen
Dunn *et al.* [10]	2-15	[-]	Abdomen
Jaqcuemoud *et al.* [23]	5.7-12.6	27-59	Forehead and arm
Nì Annaìdh *et al.* [3]	21.6 ± 8.4	54 ± 17	Back

FE simulation they fitted material parameters to biaxial tensile tests performed on human dermis strips excised from the lower back. The data used clearly shows the anisotropy of human skin, but since no method to detect the orientation of the collagen fibres was used, it was assumed that the collagen was aligned according to the Langer's lines of the lower back.

The viscoelastic properties of facial skin was investigated by Flynn *et al.* [14], [15], when they used a robot to perform highly controlled tensile deformation on multiple facial sites of several volunteers. Their study is rare as the pre-stress of the skin was calculated: *In vivo* skin does not reside in an unstressed state if void of any external load, partly due to the constant regeneration of tissue. Despite this, no widely used method of determining the pre-stress in the skin is available. Evans *et al.* [12] argue in their study that this pre-stress should have great impact on the wrinkling of skin as initiall compression of the skin would merely reduce the stress and thus not cause buckling of the surface layers.

Then *et al.* [37] also investigated viscoelastic properties of skin in their study where *in vivo* characteristics of skin were investigated using an extensometer developed at their lab which was able to perform shear tests on facial tissue. They showed that the facial skin showed clear viscoelastic properties which were also diminished if the skin was preconditioned by cyclic loading prior to testing.

Differences between men and women have been investigated in a review by Giacomoni *et al.* [17] of human skin concerning the variations between genders and through life. In the review, it is mentioned that male skin on average is thicker than female skin, while the skin thickness of both genders decreases throughout the adult part of life. Women experience a more drastic decrease than men, which is believed to be due to menopause. This thickness reduction might have to do with the simultaneous loss of collagen [17], which in turn would effect the elasticity of the skin. In a study performed by Luebberding *et al.* [29], the authors showed that there are differences between men and women throughout the major part of life in recovery of deformation. Female skin was shown to have a higher ability to recover from deformation compared to male, while male skin exhibited a higher deformation capability when tested using a suction device.

On the subject of pain, there are some that have studied the onset of a painful sensation by indenting *in vivo* human tissue using various indenters. Finocchietti *et al.* [13] utilised pressure based algometry (pain sensitivity measurements by use of a device applying a pressure to the patient) in conjunction with a FE-model to investigate the stresses throughout the soft tissue of test subjects' tibialis anterior (front muscle of the lower leg). The tests were performed on eight subjects and showed that smaller probes caused higher strains in the superficial tissue, i.e. the skin, while larger probes affected the underlying tissue to a greater degree. Moreover, values of the Pressure Pain Threshold (PPT) and the Pressure Pain Tolerance (PPTO) are stated in Table 2.4. The former indicates when the test subject experiences that the induced pressure evokes a pain sensation, while the latter indicates the pressure level at which the test subject does not want to continue the experiment.

Table 2.4: Values of the Pressure Pain Threshold (test subjects report discomfort) and the Pressure Pain Tolerance (tests subjects ask to abort) from the experiments performed in [13].

Probe type	PPT [kPa]	PPTO [kPa]
Flat probe (⌀5 mm) near muscle site	508±16	1237±51
Flat probe (⌀15 mm) near muscle site	404±24	893±25
Round probe (⌀5 mm) near muscle site	442±13	961±29
Round probe (⌀15 mm) near muscle site	272±9	653±9

The results of Table 2.4 must be regarded with caution as they are obtained from a small group of subjects and the pressures have been calculated assuming full contact between probe and skin and a homogeneous pressure distribution [13]. This is an idealisation: as shown in the work by Melia *et al.* [30] the pressure distribution may vary over the indented surface. Keeping this in mind, the magnitude of the PPT and PPTO values may be regarded as a reference to what stresses that may be reasonable when dealing with human soft tissue: As confirmed by a large study performed on citizens of Denmark at Aalborg University by Skovbjerg *et al.* [33], in which stress quantities of the same magnitude were obtained by pressure induced pain on the tibialis anterior and upper trapezius (upper back/neck) muscle. Surely the common consumer will not continue drinking if a painful sensation is felt and thus stresses reaching magnitudes of several MPa would be unfeasable during simulation of skin-like material during consumption.

Regarding the tribology of skin, Derler *et al.* [9] has compiled the results of several studies examining the friction between different sites on the body and different materials. In one of those studies a finger slid against a flat surface of polycarbonate and the coefficient of friction was found to be between 0.64 and 2.22 for dry skin and between 0.61 and 1.23 for wet skin.

Concluding Remarks

The mechanical properties of skin are: anisotropic, multilayered ([24], [32], [2]) viscoelastic ([14], [15], [37]), thus it is non-linear ([3], [38], [37], [2]). Another factor enforcing these traits is the behaviour of the collagen as with greater tensile strain in the skin the collagen fibres are straightened from their initial wound up state, thus providing strain hardening and an asymmetric load curve. It is also pre-stressed and its properties differs between persons, depending on age and sex ([38], [17], [29], [15]) while it also has intra-subject variability [27] and thus the location of the tissue may have impact on its mechanical properties.

2.3 Constitutive Equations

To define a well posed problem mathematically there are some essential parts needed as shown in Figure 2.3. One needs a geometry subject to certain Boundary Conditions (BCs) and Initial Values (IVs) which will, in the case of this thesis, require the materials within the geometry to react accordingly (through constitutive equations) to obtain equilibrium for the Partial Differential Equation (PDE) at hand being eq. (2.1).

$$div(\bar{\bar{\sigma}}) + \bar{f} = \bar{0}. \tag{2.1}$$

In eq. (2.1) $\bar{\bar{\sigma}}$ is the Cauchy stress tensor and $\bar{f}$ are all external forces acting in the material point, as this is the local form of the equation of linear momentum. To enable calculation of the stress state in the material point some constitutive equation must be supplied. The constitutive equation in this case takes the form of material behaviour and especially, since hyperelasticity is assumed, the material is set to always return to its undeformed state if void of any external load. Hyperelasticity states that there is some strain energy potential $\psi(\bar{\bar{\varepsilon}})$ which may be expressed in some strain measure $\bar{\bar{\varepsilon}}$, which provides some stress measure $\bar{\bar{S}}$ energy conjugate to $\bar{\bar{\varepsilon}}$ [1]. This can

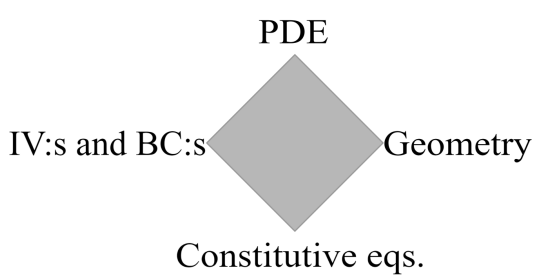

Figure 2.3: The essential parts of an FE simulation being a Partial Differential Equation, Initial Values and Boundary Conditions, a Geometry and finally Constitutive Equations.

be expressed by

$$\bar{\bar{S}} = \frac{\partial \psi}{\partial \bar{\bar{\varepsilon}}}. \tag{2.2}$$

The interested reader may consult Ottosen and Ristinmaa [35] for a detailed presentation about constitutive modelling and hyperelasticity in particular. For this work it is enough to know that finding strain energy potentials ψ modelling the facial tissue is key.

Proceeding by keeping the geometry and the boundary conditions arbitrary for the moment, simply knowing that some package is to interact with human soft tissue: Firstly the materials of interest need to be specified.

2.3.1 Material Models

Leaning on the knowledge of section 2.2, which provides specifications of material properties for skin in a broad sense properties of human soft tissue are seen in Table 2.5.

To include all of these properties will most likely produce a simulation requiring more computational effort, not to mention that a wider collection of relevant data would be needed. More data would be required since there are a great deal of studies in which human skin, even human dermis and hypodermis, are in focus: but these studies use skin from other parts of the body than the lips and facial area. Thus any data taken into consideration must be scrutinised carefully and be regarded with scepticism keeping the high intra-subject variability in mind. Moreover it is not clear how to define the direction of the collagen fibres or the strain rate dependency in the materials at hand. Consequently, idealisations are to be made regarding the material properties of human facial tissue.

The viscoelastic effects are deemed less relevant and were therefore not considered at this stage.

The multilayered property of the soft tissue may be modelled by simply using different materials for each layer and is subsequently not a requirement of the soft tissue per se. The intra-subject variability, i.e. the location dependency of the tissue is to be kept in mind, but the soft tissue material is homogeneous throughout the domain when using the selected strain energies. Age and gender dependency are also neglected.

Next, by combining the desired properties and probing literature for available hyperelastic strain energy functions, promising candidates are stated in Table 2.6.

Parameters in the various strain energies are defined in appendix A as they are not essential for the work at hand. Moreover, parameters in all the strain energy expressions share notation and thus, they will only be introduced the first time they are mentioned.

Table 2.5: The various mechanical properties of human soft tissue.

Property	**Comment**
Viscoelastic	From the high water content of the ECM and the collagen water binding ability.
Multilayered	Clear distinction between epidermal, dermal and hypodermal layers.
Anisotropic (in-planar, skin)	Clear signs of different behaviour depending on loading direction. Connected to the structure of the tissue and its collagen orientation.
Asymmetric	Strain hardened and compliant in compression
Near incompressible	From the high water content of the ECM and the collagen water binding ability.
Asymmetric load curve	High tensile strength, compliant compressive behaviour
Location dependent	Taking skin from the back of a person and comparing it with the skin from the facial area cannot be expected to behave similarly.
Gender dependent	Male and female skin have different mechanical properties.
Age dependent	The mechanical properties of skin change through life.

Table 2.6: The various mechanical properties of human soft tissue and how they may be modelled using different hyperelastic energy potentials used in literature.

Property	N-H	Ogden	GOH
Used by	[27]	[14],[15],[37],[18]	[32],[2], [37]
Anisotropic	☒	☒	☑
Non-linear $\bar{\bar{\sigma}}(\bar{\bar{\varepsilon}})$	☑	☑	☑
Near Incompressible	☑	☑	☑
Asymmetric load curve	☒	☑	☑/☒

The Neo-Hookean Strain Energy

The N-H strain energy potential takes the form of

$$\psi = C_{10}(\hat{I}_1 - 3) + \frac{1}{D_1}\left(J^{el} - 1\right)^2, \tag{2.3}$$

in which $\{C_{10}, D_1\}$ are material parameters to be set and $\hat{I}_1$ denotes the first deviatoric strain invariant, while J^{el} denotes the elastic volume ratio [1].

The Ogden Strain Energy

Writing the Ogden strain energy by use of the deviatoric stretches $\hat{\lambda}$, results in

$$\psi = \sum_{i}^{N} \frac{2\mu_i}{\alpha_i^2}(\hat{\lambda}_1^{\alpha_i} + \hat{\lambda}_2^{\alpha_i} + \hat{\lambda}_3^{\alpha_i} - 3) + \sum_{i}^{N} \frac{1}{D_i}(J^{el} - 1)^{2i}, \tag{2.4}$$

where $\{\mu_i, \alpha_i, N \text{ and } D_i\}$ are material parameters needed to be specified [1].

The Gasser-Ogden-Holzapfel Strain Energy

Define the GOH strain energy as

$$\psi = C_{10}(\hat{I}_1 - 3) + \frac{1}{D}\left(\frac{(J^{el})^2 - 1}{2} - ln(J^{el})\right) \tag{2.5}$$

$$+ \frac{k_1}{2k_2}\sum_{i=1}^{N}\left(exp[k_2\langle\hat{E}_i(\kappa, \bar{A}_i)\rangle^2] - 1\right). \tag{2.6}$$

In the definition of the strain energy, eq. (2.6), the first term may be recognised from eq. (2.3) whereas the third term is what models the collagen fibres of the soft tissue. $\{C_{10}, k_1, k_2, D, N, \kappa, \text{ and } \bar{A}_i\}$ are material parameters, where $\langle\hat{E}_i\rangle$ is a pseudo-invariant dependent on: N denoting the number of fibre families that are included, and $\bar{A}_i$ denoting the mean direction of a fibre family. For a more detailed description of the model the reader may consult [1], [32] or [37]. A number of articles have been chosen in which the Ogden, N-H and GOH strain energy is used and material data from these are presented in Table 2.7.

Table 2.7: Constitutive parameters for a selection of strain energies used in literature. I = indentation, S = suction, T = tensile. E_0, K_0, μ_0 denotes the infinitesimal elasticity modulus, bulk modulus and shear modulus respectively. Noticeable is the range or which the elastic modulus of the different strain energies span. D = Dermis, H = Hypodermis, M = Muscle and B = Bulk (no layer distinction).

Paper	Tissue	Strain energy	Area	Test	E_0 [MPa]	K_0 [MPa]	μ_0 [MPa]
[38]	D	N-H	Arm	I	6.50E+00	2.95E+01	2.22E+00
[38]	H	N-H	Arm	I	2.50E-03	3.57E-02	8.40E-04
[38]	M	N-H	Arm	I	2.15E-02	1.44E-01	7.28E-03
[27]	B	N-H	Lip	S	3.28E-02	1.44E-01	1.12E-02
[37]	H	Ogd(N=2)	Gluteus	I	5.52E-04	6.57E-02	1.84E-04
[37]	M	Ogd(N=2)	Gluteus	I	1.00E-04	2.27E-02	3.34E-05
[32]	D	GOH	Back	T	1.13E+00	-	-

Chapter 3

Human Skin Modelling

The material is one of the cornerstones in an FE-model. Thus, initially the three chosen material models, i.e: the Neo-Hookean (N-H), the Ogden and the Gasser-Ogden-Holzapfel (GOH) hyperelastic strain energies were investigated. This was done by performing single element tests where the material was exposed to both compressive and tensile strains. Initially, the material parameters were taken from articles mentioned in section 2.2. Later on, these were varied to study the effect on the material response. As the GOH material model allows for anisotropic behaviour the directional dependency was examined as a final step.

Once the material models had been examined, a material model calibration procedure took place. The calibration simulated an experiment of suction tests performed by Luboz *et al.*, their goal was to formulate material parameters by use of a suction device called LASTIC® (Light Aspiration device for in vivo Soft TIssue Characterisation). The suction device is capable of producing a controlled vacuum and measure the subsequent deformation of the material onto which it is applied. From these measurements, mechanical properties may be calculated [27]. Their experiment is useful for the calibration as it focuses on the facial area, as biological soft tissue has a variation in its mechanical properties dependent of its location on the body. Consequently, their "near lip" region measurements was used as target in the material model calibration.

Moreover, with the performed experiments Luboz *et al.* [27] formulated an FE-model, with which an inverse study to calculate N-H material parameters of the facial tissue (skin, and its underlying tissues on the geometrical site) was performed. Thus, with the aim of recreating the deformation from experiments performed in [27], a similar FE-model was created. The model was set up in ABAQUS® [1] to obtain material parameters for N-H, Ogden- and GOH hyperelastic materials through optimisation. The optimisation pro-

cess was performed using a commercial software called Isight® (©Dassault Systèmes, 2018).

The obtained materials were examined and analysed in terms of: The ability to reproduce the results in Luboz *et al.* [27], the ability to produce an expected behaviour at higher loads, the sensitivity of the material models in terms of slight adjustments to the material parameters (±10%) and finally the effects from varying the layer thicknesses. Some material configurations were thereafter discarded, and the remaining were analysed further with the help of an experiment and comparative simulations to the experiment.

The experiment consisted of applying food colouring liquid on a persons lower lip and letting that person drink from a beverage package with the A38 frame. The main area of interest were the threads and in particular how deep into the threads the food colouring liquid reached. Use of the results from the experiments and the comparative simulations one calibrated material configuration, the L2 Ogden, was chosen suitable for use in future simulations.

3.1 Method

3.1.1 Material Model Analysis

Single Element Tests

Single element tests were performed in a static analysis according to the setup in Figure 3.1. A single 1 x 1 x 1 mm quad element was used and the boundary conditions were as follows; all nodes in the XY-plane (at Z=0, i.e the far right side) were restricted in Z-direction, all nodes in the YZ-plane (at X=0, i.e the far left side) were restricted in X-direction and all nodes in the XZ-plane (at Y=0, i.e the bottom) were restricted in the Y-direction. The analyses were displacement controlled and the displacements ranged between -0.9 mm and 3.0 mm resulting in logarithmic strains between -2.3 and 1.4.

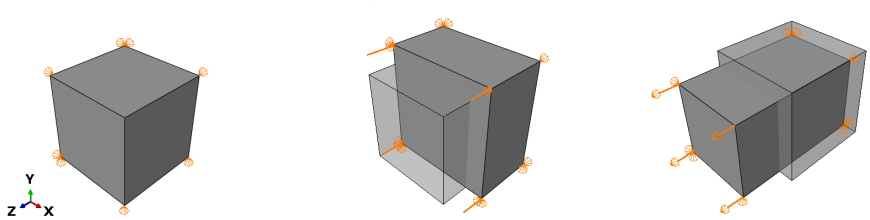

(a) Reference (b) Compression (c) Tension

Figure 3.1: Overview of the single element test setup.

Element Sensitivity Analysis

An element sensitivity analysis was done using 8-node linear brick element with reduced integration, 8-node linear brick element with full integration, 20-node quadratic brick element with reduced integration, 20-node quadratic brick element with full integration (in ABAQUS® called: C3D8R, C3D8, C3D20R, C3D20) and also using hybrid formulation for all of these four elements. The material model used in the element sensitivity analysis was the N-H material model with parameters $C_{10} = 0.0056$ and $D_1 = 3.5608$ in ABAQUS® (corresponding to a Poisson's ratio of $\nu \approx 0.49$ and an initial Young's modulus $E_0 \approx 33.7$ kPa).

Neo-Hookean

Three tests were done; one test using the mean C_{10} value from Luboz *et al.*, one test using the C_{10} value corresponding to the least stiff test subject in Luboz *et al.* [27] and one test using the C_{10} value corresponding to the stiffest test subject. The values used are presented in Table 3.1. In order for a Poisson's ratio of $\nu = 0.49$ to be held, the parameter D_1 was calculated dependent on the Poisson's ratio and the initial bulk and shear modulus of the material in line with [1] according to eq. (3.1).

$$\nu = \frac{3K_0/\mu_0 - 2}{6K_0/\mu_0 + 2} \quad , \quad \begin{cases} \mu_0 &= 2C_{10}, \\ K_0 &= \dfrac{2}{D_1}. \end{cases} \tag{3.1}$$

Substituting μ_0 and K_0 for the expressions to the right in eq. (3.1) and then solving for D_1 results in

$$D_1 = \frac{3(1-2\nu)}{2C_{10}(1+\nu)}, \quad \text{yielding } D_1(\nu = 0.49) \approx \frac{0.02}{C_{10}}. \tag{3.2}$$

Table 3.1: The material parameters used in the N-H single element tests. The comment refers either to the calculated mean, or a specific test subject, in [27].

C_{10} [MPa]	Comment
0.0032	Least stiff
0.0056	Mean
0.0076	Most stiff

Gasser-Ogden-Holzapfel

Four tests in total were done using the GOH material model examining the contributing effect of the fiber families. Three of those tests were done with two fibre families using the material parameters in Table 3.2 and one test using

Table 3.2: Material parameters used in the single element test for the GOH material model. The parameters used were taken from [32].

C_{10} $[MPa]$	D_1,[-]	k_1 $[MPa]$	k_2 [-]	κ [-]
1.007	0.020	24.530	0.1327	0.1404

the same parameters except for κ which was set to 0.3333. The tests, denoted 'Fibres XY-Plane', 'Fibres XZ-Plane, Displacement Orthogonal', 'Fibres XZ-Plane, Displacement Parallel' and their respective setup of fibre directions are shown in Figure 3.2. The test denoted 'Isotropic' had one fibre family with a density evenly distributed in all directions.

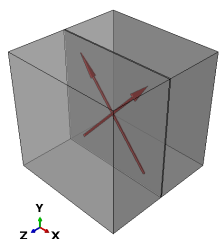

(a) 'Fibres XY-Plane'

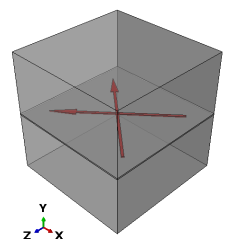

(b) 'Fibres XZ-Plane, Displacement Orthogonal'

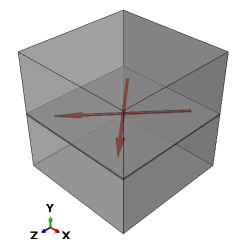

(c) 'Fibres XZ-Plane, Displacement Parallel'

Figure 3.2: Overview over the local directions used for the different setups of fibre families. The boundary conditions used were the same as described in section *Single Element Tests*.

Ogden

Five tests were done using the Ogden material model with N= 1. One test was done with the purpose of being a reference. The parameters used in the reference test were $\mu = 0.05$ MPa and $\alpha = 10.789$. Then four tests were done where μ and α were increased and decreased by 10% one at a time.

3.1.2 Material Model Calibration

Setup of the Inverse FE Simulation

The FE model for the material model calibration test was set up in ABAQUS CAE® using axi-symmetric elements with the global y-axis as symmetry axis. The dimensions of the soft tissue domain and the suction device were taken from [27]. The two parts are visible in Figure 3.3 and 3.4. The suction device was modelled as a rigid two dimensional wire part, while the soft tissue was modelled as a two dimensional shell part, which was sectioned into three distinct areas: Dermis, hypodermis and underlying muscle (Figure 3.4). This was done with the purpose of enabling the simulation to mimic facial tissue. The thickness of the two upper layers was taken from [19] and [20], while the muscle layer was set to fill the remainder of the domain for the purpose

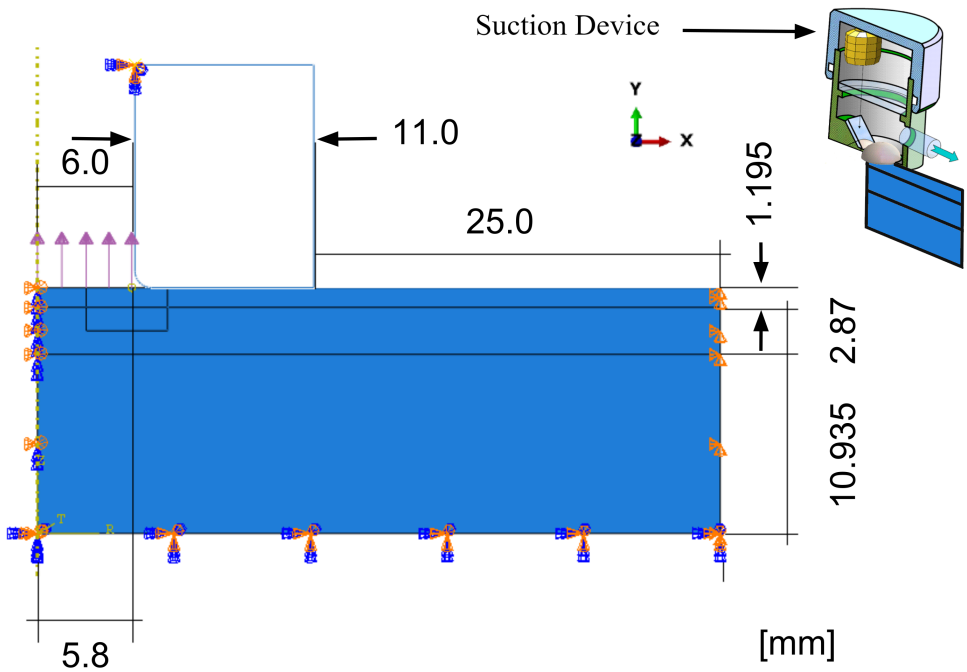

Figure 3.3: The assembly of the soft tissue slab with the applied load and boundary conditions being marked in the figure.

of being able to keep a comparable domain as to [27]. The thickness of the various layers is reported in Table 3.4.

Meshing was performed such that it was most detailed close to the rounded corner (left lower point) of the suction device, so as to better capture the contact between it and the soft tissue. 188 RAX2 elements were employed for the rigid suction device while for the soft tissue 2781 CAX8R elements were used. The CAX8R are quadrilateral eight node elements using reduced integration [1]. To evaluate the impact of element choice and of mesh density a mesh convergence study was performed. The output to study convergence was the maximum displacement of the *center node* (Figure 3.4), as well as maximum von Mises stress in the elements subjected to the negative pressure. Moreover, the required simulation time was also taken into account.

Furthermore, the nodes situated on the right border of the soft tissue slab were pinned in all directions. Nodes on the left border, being coincident with the symmetry axis of the full soft tissue domain, were only allowed to move in the Y-direction and rotation about the Y-axis was restricted as well. Lastly the bottom border and the suction device had all degrees of freedom locked (see Figure 3.3). Contact between the suction device and the soft tissue was modelled using the built in general contact which modelled the suction device and the tissue to move frictionless to each other tangentially while employing hard contact in all normal interaction. The vacuum created

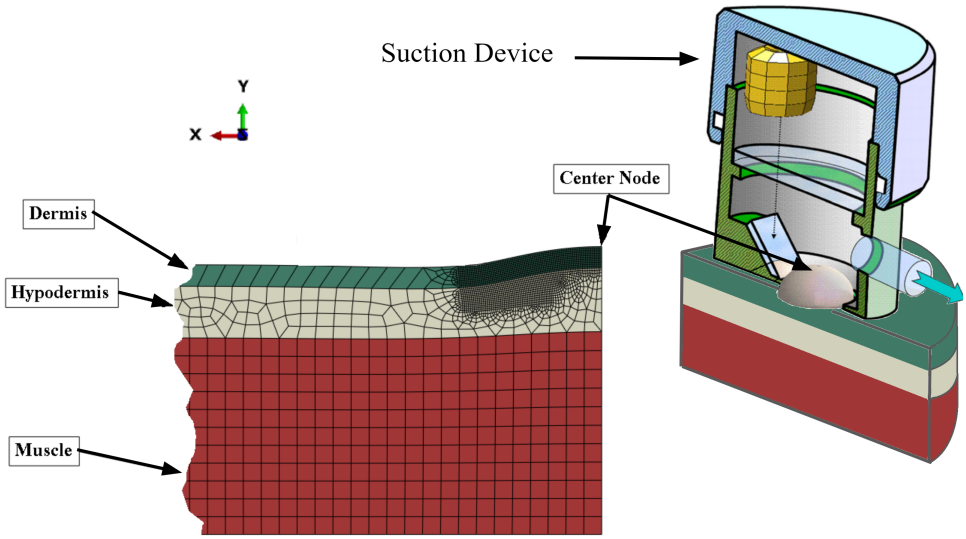

Figure 3.4: To the left is the soft tissue slab and its mesh, which is refined close to the suction device edge, also visible is the sectioning of the tissue layers. To the right is the suction device being cut in the center plane, showing the suction compartment. Additionally the center node is marked.

by the suction device was modelled as a negative pressure influencing the upper edge of the soft tissue amounting to a total of 7.3 kPa as maximum pressure [27] (seen in Figure 3.3 as the line marked with purple arrows). The pressure was set to ramp during the step. The simulation was performed using static analysis in ABAQUS®. Output was generated for the center node Y-displacement.

Material Parameter Calibration

Four different configurations of material models and number of material layers were defined denoted 'L1', 'L2 GOH', 'L2 Ogden' and 'L3'. L1 comprised of a single homogeneous layer using the N-H material model. L2 GOH comprised of two layers, one outer layer using the GOH material model representing the dermis and one bulk layer using the N-H material model representing the soft tissue bulk material. L2 Ogden were similar to L2 GOH with the difference being that the dermis was represented by the Ogden material model instead. L3 were similar to L2 GOH with the exception that the bulk layer were divided into two N-H material models with the purpose of representing the hypodermis and muscle tissue.

Representations of the configurations are shown in Figure 3.5. Initial guesses for the different material model parameters were taken from [27], [32] and [38]. A summary of the configurations, initial guesses and also the limits can be seen in Table 3.3. The optimisation was performed using Isight® by

minimising the error between the target vector, being the displacements vs. pressure, from Luboz's experiments and the corresponding output from the simulation when altering the material parameters in the different configurations. Thus, matching the Y-displacement of the center node as a function of the applied pressure, for each configuration, with the mean result in Luboz's experiments.

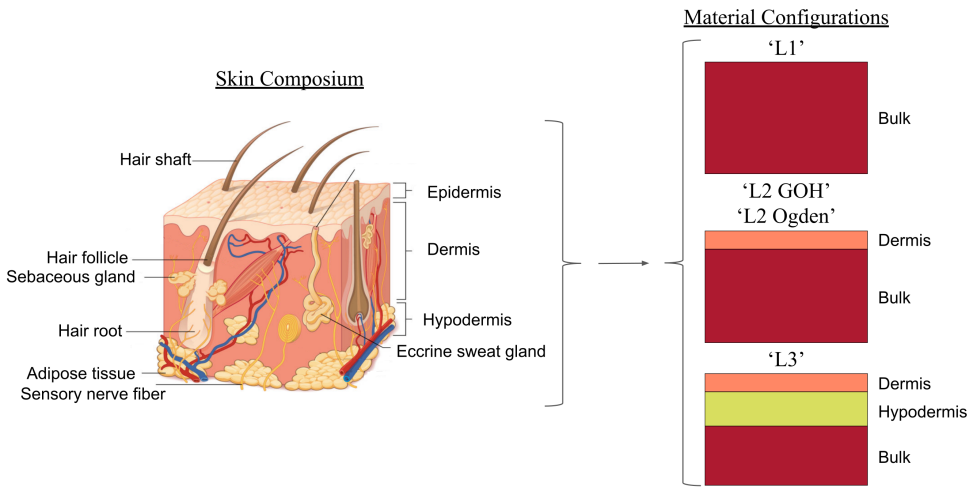

Figure 3.5: A picture of a figurative piece of skin with the three tissue configurations L1, 'L2' and L3 shown to the right. The left part has been reworked from [7]

Table 3.3: Different configurations of number of layers and material models used in the optimisation process (C_{10} [MPa], k_1 [MPa], k_2 [-], μ_1 [MPa], α_1 [-], LL = Lower Limit, IG = Initial Guess, UL = Upper Limit).

Config.	Tissue	Mtrl. model	Param.	LL	IG	UL
L1	Soft tissue	N-H	C_{10}	0.0014	0.0056 [27]	0.0224
L2 GOH	Dermis	GOH	C_{10}	0.025	0.1007 [32]	0.4028
			k_1	6.1325	24.53 [32]	98.12
			k_2	0.033175	0.1327 [32]	0.5308
	Soft tissue	N-H	C_{10}	0.0014	0.0056 [27]	0.0224
L2 Ogden	Dermis	Ogden	$\mu 1$	0.005	0.0113 [18]	0.05
			α_1	2.5	10.808 [18]	15.0
	Soft tissue	N-H	C_{10}	0.0014	0.0056 [27]	0.0224
L3	Dermis	GOH	C_{10}	0.025	0.1007 [32]	0.4028
			k_1	6.1325	24.53 [32]	98.12
			k_2	0.033175	0.1327 [32]	0.5308
	Hypodermis	N-H	C_{10}	0.000105	0.00042 [38]	0.00168
	Muscle	N-H	C_{10}	0.00091	0.00364 [38]	0.01456

Using the optimised parameters a simulation was performed for each material model configuration in which the suction was increased to 12.0 kPa, 21.9 kPa, 17.5 kPa, 21.9 kPa for L1, L2 GOH, L2 Ogden and L3 respectively.

Layer Thickness Sensitivity Analysis

A layer thickness sensitivity analysis was carried out for L2 GOH, L2 Ogden and L3 using the optimised material parameters. For both L2 GOH and L2 Ogden the thickness of the dermis was varied and for L3 also the thickness of the hypodermis was varied. The magnitudes of the variations are reported in Table 3.4.

Table 3.4: Layer thickness variations in the layer thickness sensitivity analysis where the values of the dermis are taken from [19] while values for the hypodermis are taken from [20].

Tissue	Thin [mm]	Standard [mm]	Thick [mm]	Variation
Dermis	0.7851	1.195	1.6044	$\pm$ 2 STD
Hypodermis	1.55	2.87	4.19	$\pm$ 2 STD

3.1.3 Material Model Validation

Experiment

Red food colouring liquid was applied on the test subject (female, age 26) lower lip. She was then asked to drink from a beverage package with the A38 opening device in a normal fashion. The A38 was chosen because it has more threads than the DC. Afterwards, photos were taken of the package from the front and also two photos were taken of the threads obliquely from above and from below. Then, more colouring was added on the test subjects lower lip and the test subject was asked to press, using relatively high force (without experiencing any discomfort), the side of the frame against the lower lip. Then, a photo was taken of the package opening from the front.

Simulation

A FE model was set up as seen in Figure 3.6. The lip was modelled with dimensions according to Figure 3.6 and boundary conditions used were that the lower side of the lip was restricted in X- and Y-direction. The upper side of the package part was constrained using coupling to a reference point which were not allowed to rotate or move in the X-direction. During the simulation the package neck was pressed down into the lip until the reaction force in Y-direction acting on the reference point of the package part reached 0.3 N. Two simulations were performed, one with L2 GOH and one with L2 Ogden.

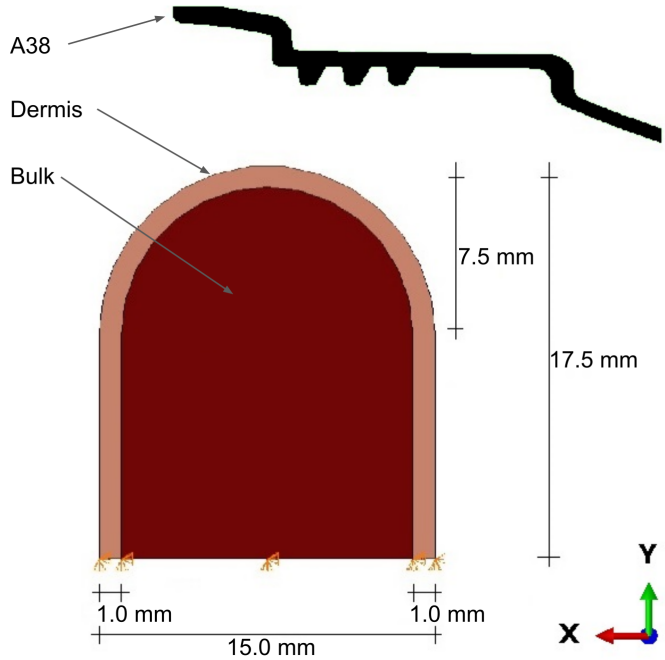

Figure 3.6: Setup of the virtual model for the validation test.

3.2 Results and Analysis

3.2.1 Material Model Analysis

No difference in the stress-strain response could be observed in the simulations regardless of element choice during the single element tests.

Neo-Hookean

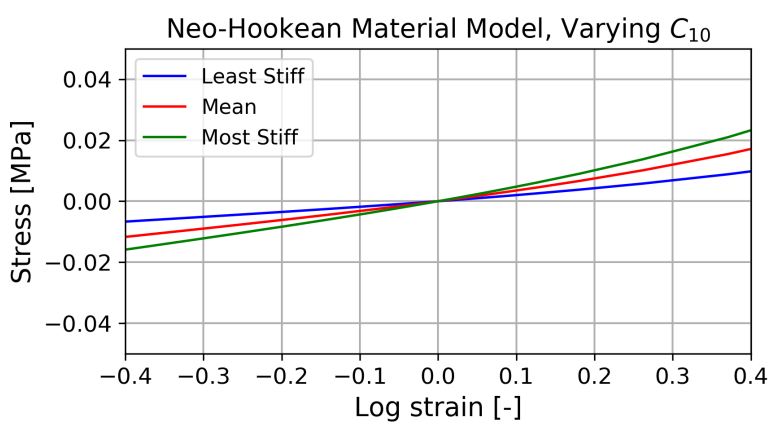

Figure 3.7: Single element test results for when varying C_{10} in the N-H material model.

In Figure 3.7 the results from varying the C_{10} parameter of the N-H material are displayed. For the employed C_{10} values the N-H model behaves almost linear within the mean failure strain stated in [3]. This does not reproduce the expected behaviour of a three phase curve in Figure 2.2. However as the test in Luboz *et al.* [27] is done for small deformations and the N-H material model does not have a term representing the collagen fibers this is expected.

All of the lines lie well below the ultimate tensile strength values reported in Table 2.3 when the mean failure strain of $\approx 50\%$ (engineering strain) is reached. This means that the N-H model is only valid for small deformations and is therefore not a suitable choice for representing the dermis during the optimisation process.

Gasser-Ogden-Holzapfel

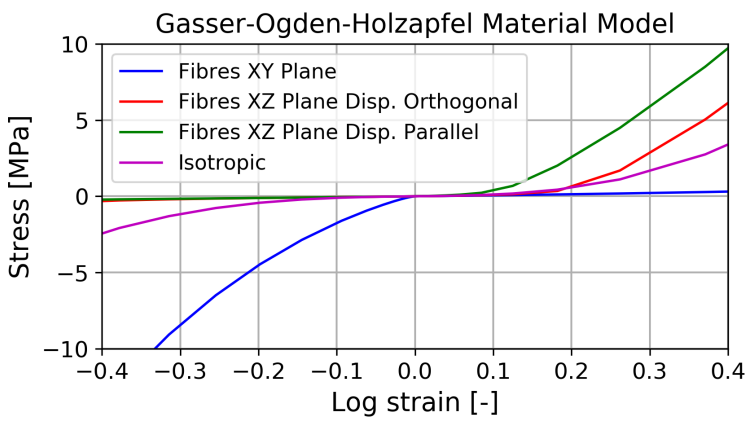

Figure 3.8: Single element test results for the GOH material model for four different fibre family configurations.

Single element tests of the GOH material and the dependency of fibre directions are found in Figure 3.8. The order from stiffest to least stiff fibre direction in tension is 'Fibres XZ Plane, Tension Parallel' (i.e when the fibre families' local directions reside in the XZ plane and the axis they deviate from is parallel to the Z direction), 'Fibres XZ Plane, Tension Orthogonal' (i.e when the fibre families local directions lie in the XZ plane and the axis they deviate from is orthogonal to the Z direction), 'Isotropic' and 'Fibres XY Plane (i.e when the fibre families' local directions lie in the XY plane). This is not surprising as the stiffest behaviour should be obtained with the configuration with local directions aligning with the Z direction.

The 'Fibres XY Plane's compliant response is a consequence of the elongation of the single cube element in the Z direction. Due to the near-incompressible behaviour this causes shrinkage in both the X- and Y direction, which com-

presses the fibre families. When looking at the compressive side of Figure 3.8, the same mechanism causes elongation in both X and Y direction thus activating the fibre families, when the cube element is compressed in the Z direction. Making this configuration the stiffest in compression.

One could expect that the 'Isotropic' configuration would have the same response in tension and compression since the fibre density is evenly distributed in all directions. However, this is not the case as seen when comparing the tension and compression part of the curve. This is because one of the terms in the GOH strain energy (eq. (2.6)) is the N-H model (eq. (2.3)), which does not give the same response in tension and compression.

The overall behaviour corresponds quite well with the three phase behaviour mentioned in the literature; first an initial phase where low loads correspond to large deformations, secondly a phase of stiffening and lastly a stiff almost linear response. This together with the possibility of an anisotropic behaviour makes the GOH model a suitable candidate for representing the dermis. However, as the choice has been made to assume the material as isotropic, if the GOH material model is to be used the fibre family density will be distributed evenly in all directions.

Ogden

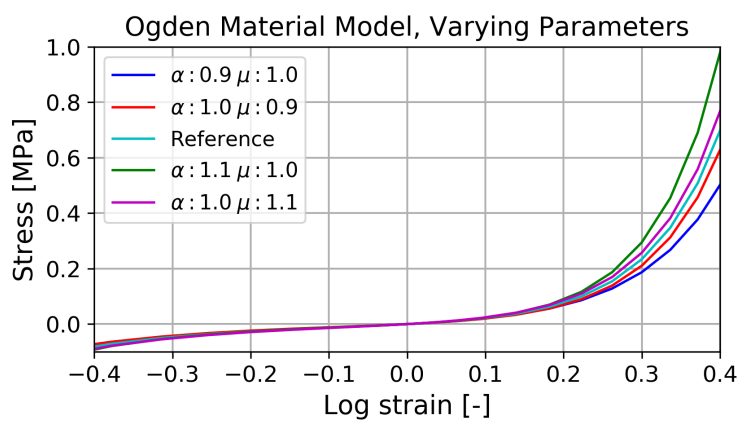

Figure 3.9: Single element test results for when varying μ and α in the Ogden material model.

A study of the material parameter dependency in the Ogden material is seen in Figure 3.9. Two things are noticed directly. The compliant response during compression and the hardening response during tension. This is desired responses, which means that the Ogden model is a suitable candidate. The limitation of this material model is that it can not reproduce the anisotropic behaviour of the dermis. However, this is not a problem in this thesis. When studying the effects of varying the material parameters it is seen that it mostly

affects the tensile response.

3.2.2 Material Model Calibration

Mesh Convergence for the Material Calibration Test

By varying element density and element type in the simulations, the results seen in Figure 3.10 were obtained. It is clearly visible that the displacements in a) converges more quickly than the maximum von Mises stress. This seems natural as the stress response of the structure is dependent on the gradient of the displacements. The cost of refining the mesh is visible in b), where the total CPU time reported for each element type is relative to the CAX4RH element simulation. Notable is the strong connection between CPU time and increasing number of nodes in the simulation: Be it either by increasing the mesh density, i.e. the number of elements in the domain, or by increasing the order of the elements, which doubles the nodes per element.

Elements using hybrid formulation require slightly more time to finish the

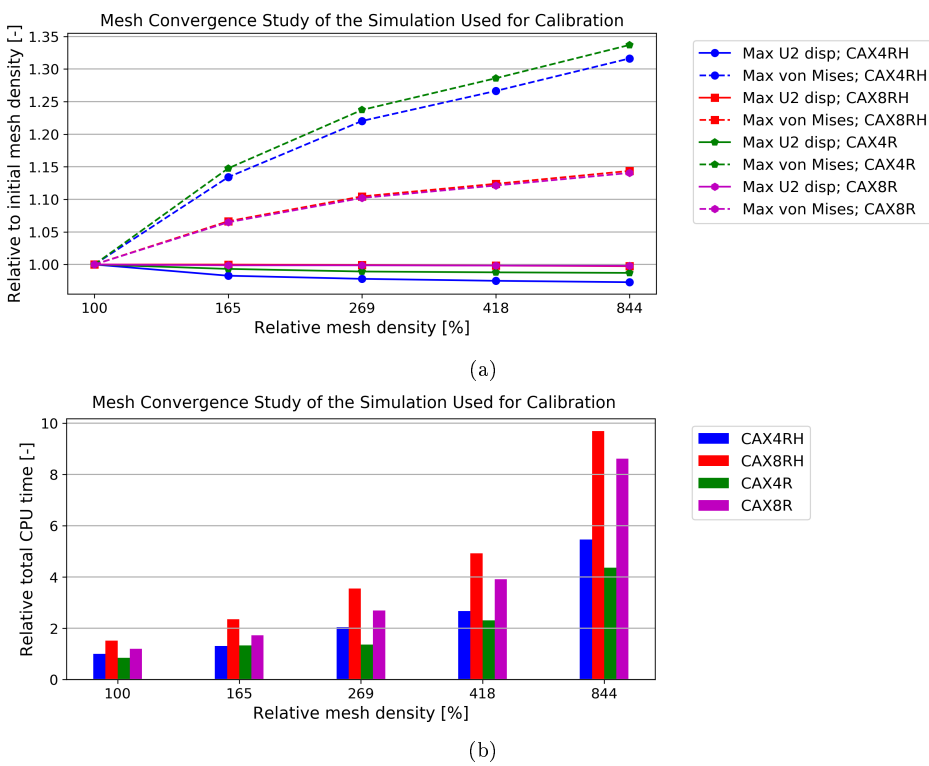

Figure 3.10: Results from the mesh convergence study of the 2D material calibration test. a) the maximum von Mises stress in the elements subjected to the external load, as well as the maximum Y-displacement of the center node relative to the coarsest mesh of each corresponding element type. b) the total CPU time relative to the coarsest mesh for the CAX4RH element which was 52.64 s.

calculations than the elements using the conventional formulation (Figure 3.10b). It is not known why this is, but it should have to do with the different ways of calculating the stress, as the hydro-static pressure is calculated in a different manner for hybrid elements.

Due to the nature of the load case of the simulation used to calibrate the material models being dominated by bending of the elements, it was decided that second order elements be used instead of first order elements. Firstly fully integrated first order elements are known to demonstrate shear-locking, i.e. too stiff behaviour by letting energy be stored by shearing the elements excessively. Secondly reduced integration elements can handle the shear-locking behaviour, while they instead allow certain deformation modes of the elements not resulting in any strain energy being detectable in the element-so called hourglassing [1]. To overcome both these difficulties, second order reduced integration elements were used. Moreover, the middle option using $\times 2.69$ the elements of the coarsest mesh resulting in 2781 elements as the von Mises stress were then converged within a 5% error margin, and the displacements to a 2.5% error margin of the asymptotic trend of the CAX8R graphs (Figure 3.10a) while still retaining a reasonable computational time (142 s).

Material Parameter Calibration

Table 3.5: Optimised parameter values for the different configurations and material models used in the calibration process (C_{10} [MPa], k_1 [MPa], k_2 [-], μ_1 [MPa], α_1 [-], IG = Initial Guess).

Config	Tissue	Mtrl. model	Param.	IG	Opt.	Change
L1	Soft tissue	N-H	C_{10}	0.0056	0.0049767	-11%
L2 GOH	Dermis	GOH	C_{10}	0.1007	0.025	-75%
			k_1	24.53	24.491	-0.2%
			k_1	0.1327	0.1327	0%
	Soft tissue	N-H	C_{10}	0.0056	0.0041867	-25%
L2 Ogden	Dermis	Ogden	μ_1	0.0113	0.05	+343%
			α_1	10.808	10.789	$\approx$ 0%
	Soft tissue	N-H	C_{10}	0.0056	0.004292	-23%
L3	Dermis	GOH	C_{10}	0.1007	0.025	-75%
			k_1	24.53	24.492	-0.2%
			k_1	0.1327	0.13265	$\approx$0%
	Hypodermis	N-H	C_{10}	0.00042	0.00168	+300%
	Muscle	N-H	C_{10}	0.00364	0.011334	+211%

The results from calibration of the chosen configurations are displayed in Table 3.5. Looking at the 'Change' column it is seen that the C_{10} parameter for L1 decreased by 11%. Since the initial guess for that parameter is taken from [27] it would not change in a perfect setting given that the simulations are to be identical. However since there could be small differences in the setup of our CAE model and the one formulated in [27], this change is not

surprising. Furthermore, the length of our target vector (i.e. up to which pressure the simulation was performed) used in the optimisation process most likely affected the obtained parameter values. With this said, the change of 11% falls well within reasonable limits, since the least stiff patient in [27] resulted in a parameter value of $C_{10} = 0.0032$ and the stiffest resulted in $C_{10} = 0.0076$.

Moving on to the changes for L2 GOH, the 75% decrease for C_{10} in the GOH material model is not considered unreasonable since it is between the C_{10} value of 0.00186 found in [37] and 0.1007 found in [32]. The k_1 and k_2 were barely changed and is therefore not commented upon. The decrease for the C_{10} in the N-H layer is considered reasonable since it falls within the results in [27].

Examining the changes for the parameters in the L2 Ogden configuration, it is seen that the μ_1 term increased by $\approx 300\%$ to 0.05 MPa. As this corresponds to an initial Young's modulus of ≈ 149 kPa for a nearly incompressible material, the change is considered reasonable. The optimised C_{10} for the bulk layer is almost the same as for the L2 GOH configuration and is therefore deemed reasonable.

Looking at the parameter changes for L3 it is seen that the GOH parameters are practically the same as for L2 GOH but the parameters of the N-H layers have increased between $200 - 300\%$. This raises the suspicion that the three-layer configuration's mechanical response could be very sensitive to variations in layer thicknesses.

Figures 3.11-3.13 show the calibrated material configurations fit to the target vector used in the optimisation process. The two latter ones also show the highest tensile and compressive strains present in the dermis layer. All four configurations display good fits to the target vector. The R^2 values differ on the third and fourth decimals from an otherwise perfect fit (i.e $R^2 = 1$). The minimum and maximum strains present in the dermis for L2 GOH and L2 Ogden are within realistic limits (Figures 3.12 - 3.13).

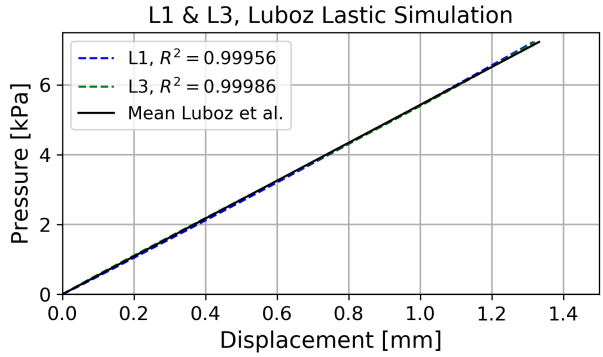

Figure 3.11: The calibrated L1 and L3 material configurations' performance with the Luboz LASTIC® test [27] (Mean Luboz et al.) as target vector.

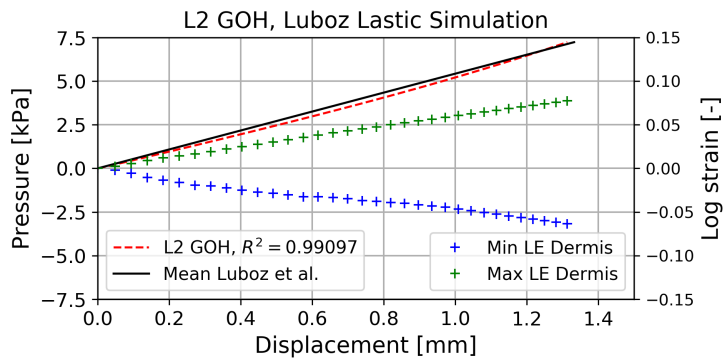

Figure 3.12: Simulation of the Luboz LASTIC® test, using the calibrated L2 GOH material configuration. The blue and green crosses represent the dermis minimum and maximum principal logarithmic strain respectively.

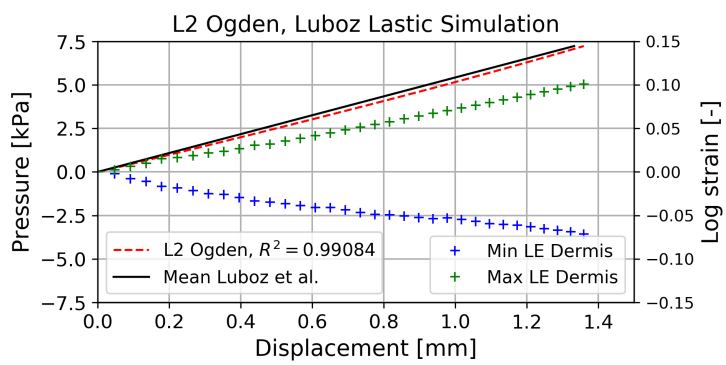

Figure 3.13: Simulation of the Luboz LASTIC® test, using the calibrated L2 Ogden material configuration. The blue and green crosses represent the dermis minimum and maximum principal logarithmic strain respectively.

Figure 3.14 shows the behaviour of the calibrated material configurations

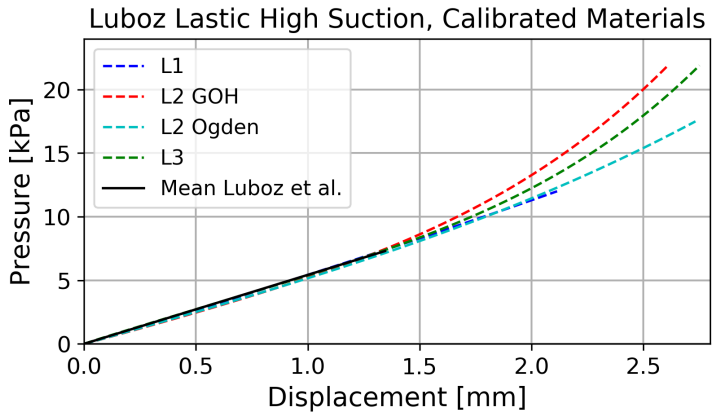

Figure 3.14: Simulating the Luboz LASTIC® test for higher negative pressure than in the test. The solution for L1 did not converge over $\approx$ 12 kPa and the solution for L2 Ogden did not converge over $\approx$ 17.5 kPa.

when the suction is increased. L1 continues to behave linearly up to 12 kPa suction, while L2 GOH and L3 show non-linear behaviour. This is not surprising since L1 lacks the behaviour of the fibres provided by the exponential terms in the GOH material model used in the other two configurations. It may also be noted that L2 GOH and L3 do not differ from each other substantially, making both a potential choice. Lastly, the L2 Ogden configuration shows slight deviation from the linear curve of the experiment, which could indicate a more compliant material behaviour than what is expected.

Layer Thickness Sensitivity Analysis

By varying the thickness of the different soft tissue layers the resulting displacement vs. pressure graphs are seen in Figures 3.15-3.17, for the L2 GOH, L2 Ogden and L3 in that order.

As the material parameters used for the N-H bulk layer practically are the same for both L2 configurations (The C_{10} used in the L2 GOH and the L2 Ogden corresponds to an initial Young's modulus of $E_0 = 25.1$ kPa and $E_0 = 25.8$ kPa respectively) it is safe to assume that the dermis layer constitutes the reason for the differences in the mechanical response. When comparing Figure 3.16 and Figure 3.15 it is seen that the L2 Ogden configuration is less sensitive to thickness variations of the dermis layer than the L2 GOH configuration. Another difference is that the L2 GOH configuration shows a more pronounced non-linear behaviour (it stiffens very rapidly most likely originating from the fibre term in the strain energy expression). The fact that the experimental results in Luboz *et al.* [27] exhibit an almost linear behaviour for these small deformations speaks against further investigating the L2 GOH configuration. However, it should not yet be discarded.

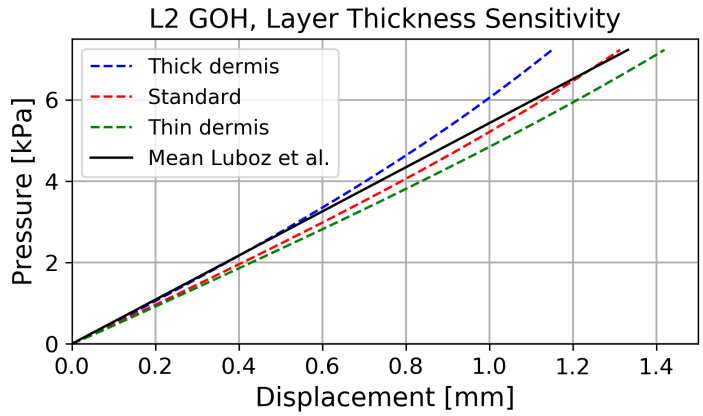

Figure 3.15: Pressure vs. displacement of the center node from the variation of layer thickness for the L2 GOH material configuration.

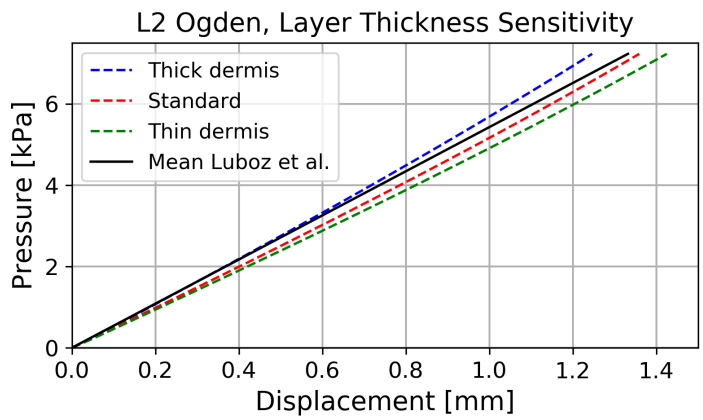

Figure 3.16: Pressure vs. displacement of the center node from the variation of layer thickness for L2 Ogden material configuration.

Studying Figure 3.17 it is seen that the three-layer configuration shows large variations in the mechanical response when layer thicknesses are varied. As stated previously, this was suspected. The L3 configuration is chosen not to be further investigated mainly due to two reasons: Firstly, the lack of information regarding which tissues are the most dominant in a real life setting makes it hard to make an assessment of the credibility of the result. Secondly, the fact that, if used, the hypodermis layer will be drawn by hand for the 2D simulations, one can easily imagine what impact a slightly misplaced spline control point could have on the mechanical response of the lip structure.

Material Parameter Sensitivity Analysis

The results from varying the material parameters of the different configurations may be seen in Figure 3.18 and 3.19. The naming convention employed

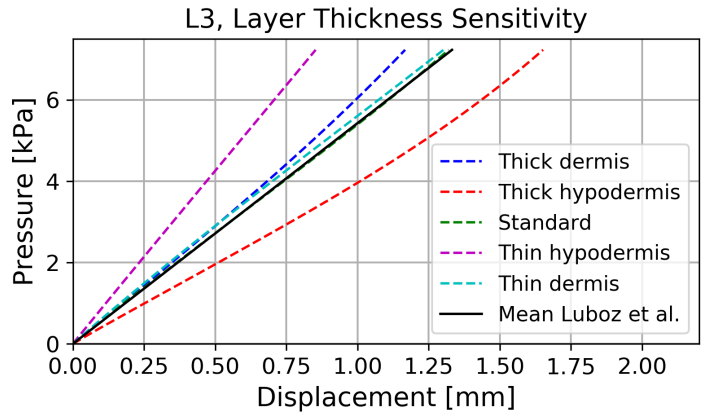

Figure 3.17: Pressure vs. displacement of the center node from the variation of layer thickness for L3 material configuration.

is that of '<configuration name>_<Percentage of the standard><Parameter Name>'. Simulations using the optimised material parameters from Table 3.5 are named '<configuration name>_<standard>'. The material parameters of the different configurations may be seen in equation (2.3) and (2.6) on page 16. The bulk material is referred to as subdermis in the legends.

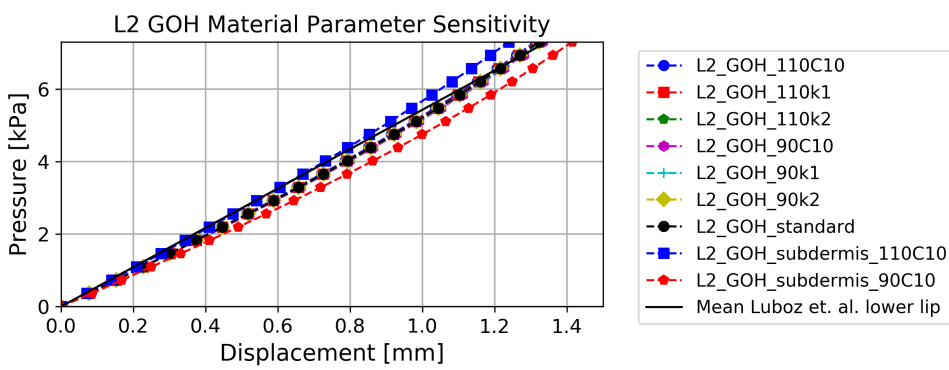

Figure 3.18: The effect of varying the material parameters ±10% for the L2 GOH configuration. Note the dominant impact on compliance from the subdermis layer when its parameters are varied, while variation of the dermis' parameters barely change the compliance at all.

Reviewing Figure 3.18 and 3.19 none of the different configurations display an unstable behaviour. The most stable configuration is the L2 GOH in Figure 3.18, which barely changes at all when altering the material parameters. Looking instead at Figure 3.19 changing the parameters of the bulk material creates a noticeable impact on structural behaviour, causing decreased compliance for a 10% increase of the C_{10} value of the underlying N-H material, and vice versa when the same parameter is decreased. This should be expected since the bulk material for the two layered models constitutes the

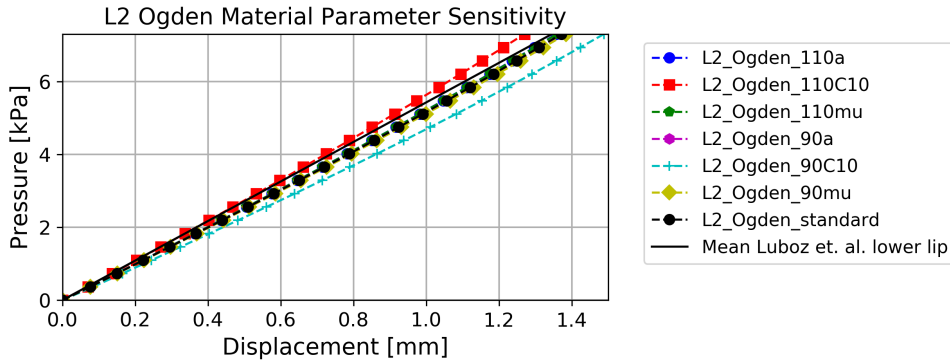

Figure 3.19: The effect of varying the material parameters ±10% for the L2 Ogden configuration. The subdermis layer constitutes the majority of the change to the compliance when its parameters are varied, while the parameters of the dermis have low effect.

majority of the soft tissue domain and thus alteration of this material should also significantly impact the bulk behaviour. Change in the material parameters of the Ogden material displays no aggressive change of the fit to the target vector, implying that the minima found during optimisation is stable in its surrounding. Comparing the resulting L2 Ogden dermis material with experimental data a reasonble fit is shown (Figure 3.20).

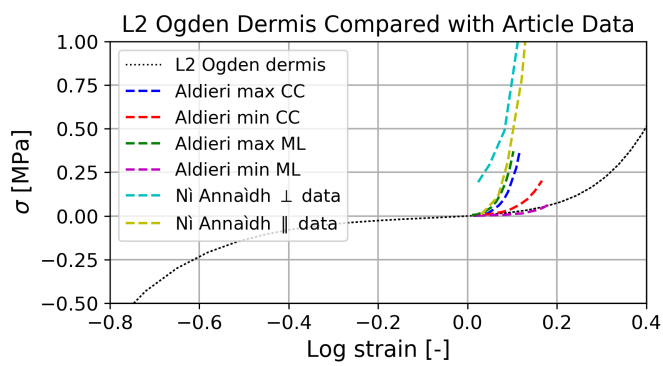

Figure 3.20: The L2 Ogden dermis material compared to article data taken from Nì Annaídh *et al.* [32] (direction is relative Langer's lines) and Aldieri *et al.* [2] (CC being CranioCaudal = axis from head to feet, and ML being Medio Lateral = axis from nipple to nipple).

3.2.3 Material Model Validation

Evaluating the material configurations for the application in mind, the experimental tests are seen in Figures 3.21-3.22.

Drops of food colouring liquid can be clearly seen when examining Figure 3.21 and Figure 3.22. It can also be seen that more food colouring has gathered at the inner edges than on the flat surfaces. This is believed to be

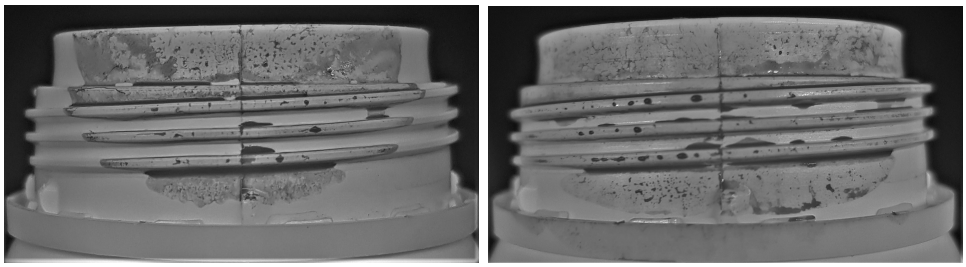

(a) Neutral Pressure (b) High Pressure

Figure 3.21: Photo from the front of the A38 after neutral and high drinking pressure had been applied using the liquid colouring.

because of gravity and or capillary action. Both of these are considered as disturbances. The fact that people are of different sizes and drink differently, together with the fact that the experiment was only performed one time with one person, makes it challenging to analyse the size of the contact area in more detail.

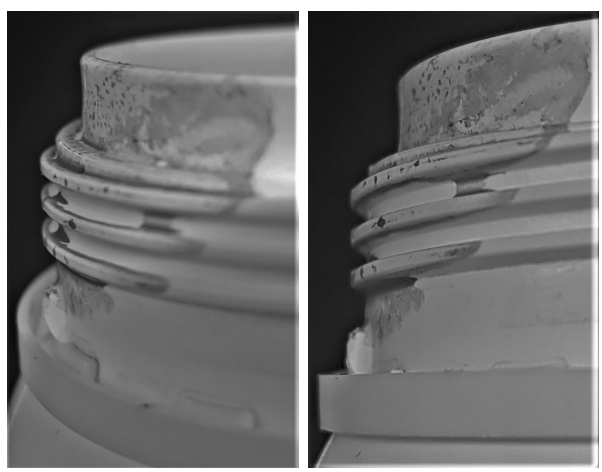

(a) (b)

Figure 3.22: a) Photo from the upper right side of the A38 after normal drinking pressure had been applied. b) Same as (a) except from the lower right side.

The deformation pattern around edges and threads was the main area of interest for the experiment and some conclusions can be drawn when looking at Figure 3.22 in particular. The contact area stretches all the way from the opening to a couple of millimetres below the lowest thread with the exception that no contact took place at the root of the threads. This indicates a rather compliant behaviour of the lips.

Figure 3.21(b) shows that even if the package was applied with, in the context, high force no contact took place between the lips and the root of the threads. This provides a rule of thumb for when assessing the credibility of

the simulations. A lot of the disturbances probably originate from the solvent used not being viscous enough. More accurate results should be able to be obtained by using another way to apply the colour to the frame, for instance lipstick or coloured sugar syrup.

Pictures of the deformations are seen in Figure 3.23, while contact between the opening device and the soft tissue domain are superposed on the experimental results in Figures 3.24-3.25.

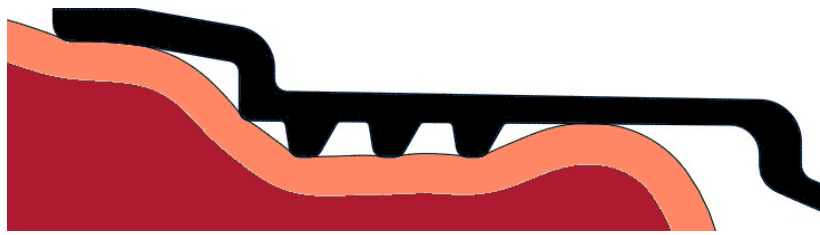

(a) L2 GOH

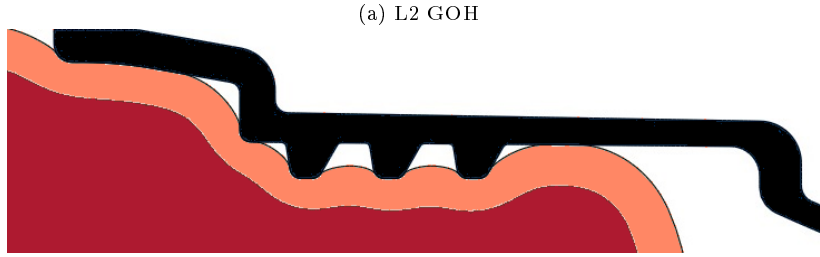

(b) L2 Ogden

Figure 3.23: Simulation results when pressing the A38 neck against the lip with 0.30 N.

Comparing the simulations to the experiments, noting that the applied force during the experiment was not measured, it cannot be known if the magnitude of the forces were the same in the experiment and the simulations. However, the force was approximated as being one tenth of a 3 dl beverage package multiplied with the gravitational acceleration, i.e ≈ 0.3 N. This approximation was based on the thought that the hand does not bear up all the weight of the package when drinking.

When comparing Figure 3.23(a) with Figure 3.23(b) it is seen that the L2 GOH configuration is stiffer and less compliant around edges than the L2 Ogden configuration.

Studying Figure 3.24(a) and (b) and in particular analysing the crest of the threads it is noticeable that the L2 Ogden better resembles the experimental results. Continuing, looking at Figure 3.25(a)-(d) it is quite clear that also in the focus of contact area the L2 Ogden configuration better resembles the experimental results.

With these results as motivation: the material configuration chosen for further use was the L2 Ogden configuration, as it displayed the best overall perfor-

mance. Both taking into account the calibration test and also the contact behaviour when being indented with a package frame.

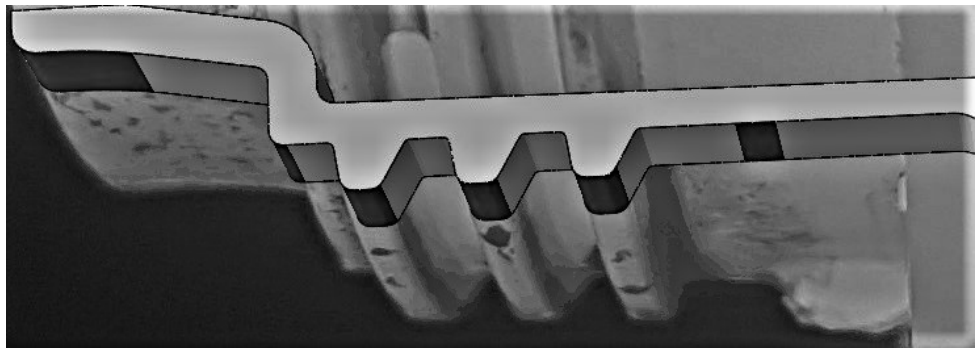

(a) L2 GOH

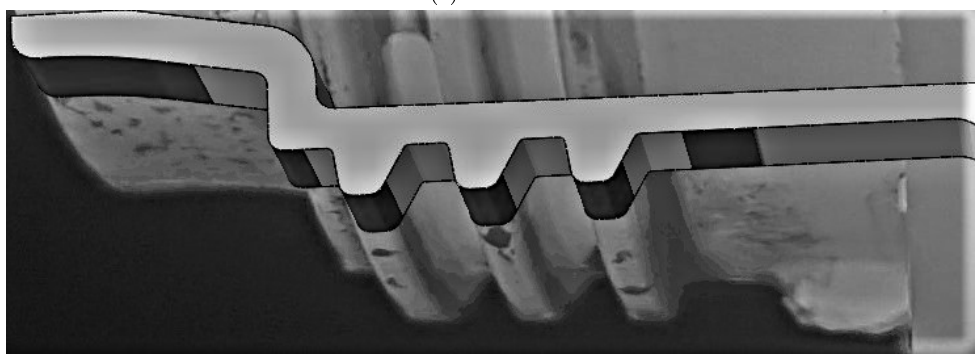

(b) L2 Ogden

Figure 3.24: Comparison between experimental results and simulation.

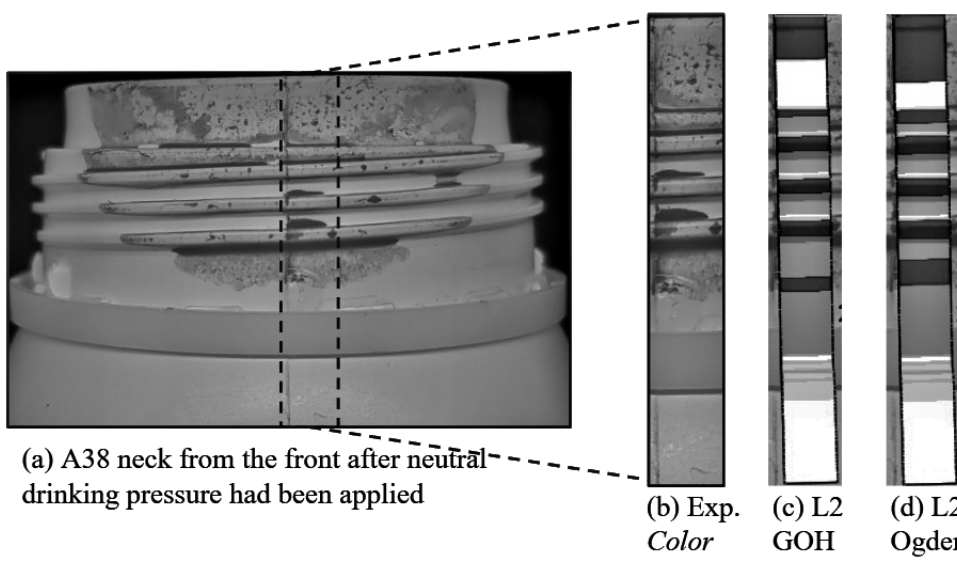

Figure 3.25: Comparison between experiment results and simulations for the two L2 materials.

Chapter 4

Drinking Sequence Modelling

Using the calibrated material configurations from chapter 3 simulations of the drinking action both in 2D and in 3D have been performed.

For the 2D simulations real life drinking sequences were recorded and the movements of the head and packages were extracted from the recordings. The movements were then used as displacement BCs in the 2D simulations, for both the opening devices (Figure 1.1, p.4). The scenarios depicted were of a newly opened package and of a package that was almost empty.

Then the step into 3D was made: introducing a three dimensional human head (Figure 4.1). The geometry, abbreviated MIDA (Multi-modal Imaging based Detailed Anatomical model), is that of a head scanned from the neck and up. The model and all data connected to it has been produced in a collaboration between the Food and Drug Administration's (FDA, `https://www.fda.gov/`) Center for Devices and Radiological Health and The Foundation for Research on Information Technologies in Society (IT'IS, `https://itis.swiss/who-we-are/`).

(a) MIDA (b) Skin (c) Muscle

Figure 4.1: Different tissues available in MIDA, which is especially useful as all tissue has previously been professionally sectioned. The figure is part of an image present in [21].

The final surface mesh of the head has been acquired from MRI imaging using semi-automatic segmentation of the various tissues combined with a

subsequent procedure to refine the segmented tissue into non-self-intersecting surfaces. Sampling of the head was performed by a maximum of 500 μm isotropic voxel size. For a more detailed description, the reader is referred to the article written in conjunction with the publication of the model [21].

Simulations were then performed using data from the licensed model to reproduce a realistic facial domain that interacted with the package opening devices during dynamic analyses.

Methods of drinking

According to information provided by Tetra Pak®, the method people use when drinking from a package can roughly be divided into three different styles; 'Suck', 'Pour' and 'Pull' (Figure 4.2). When using 'Suck', the individual creates a complete seal between the lips and the package and control the flow using vacuum. When using 'Pour', the person does not create a seal but simply control the flow using gravity by tilting the package. 'Pull' is a mixed method, when using this method a person embraces the package with the lower lip whilst the upper lip seals with the liquid. The flow is then controlled using both gravity and vacuum.

(a) Suck (b) Pour (c) Pull

Figure 4.2: Illustration of the three most common ways of drinking from a package. The images are a courtesy of Tetra Pak™.

4.1 Method

4.1.1 Drink Sequence Motion Capture

Post-it notes were cut down into quadratic pieces with a side length of roughly 1 cm. A black dot was applied at the centre of each piece and four pieces were applied on the face of the test subject (male, age 29). Also two black markers were made on the neck of the frame both on the A38 and on the DC frame (Figure 4.3). Then the test subject was asked to drink from the package and the motion was recorded using a Canon 650D digital single lens reflex camera mounted on a tripod.

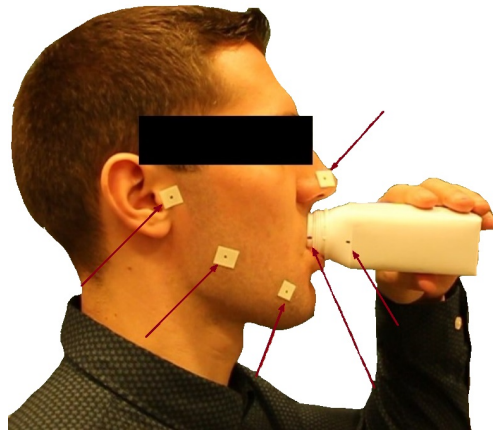

Figure 4.3: Overview of the markers used in the motion capture.

Four scenarios were recorded and each scenario was recorded two times. The four different scenarios were 'A38 F', 'A38 AE', 'DC F' and 'DC AE' where 'F' and 'AE' means 'Full' and 'Almost Empty' respectively. The most suitable movie (depending on e.g that the markers were visible in all frames) of each scenario were then loaded into Mediaview (Altair® Engineering, Inc.). Using Mediaview (x,y)-coordinates for the two markers on the packages, the marking on the nose and the marking on the ear were extracted from movie at selected frames (frames corresponding to the moment just before contact until let go).

The two markers on the lower jaw were not used because the markers did not follow the motion of the lower jaw, as the skin of the cheek slid over the jawbone. The (x,y)-coordinates were then processed re-scaling them from pixels to mm and calculating the translation and rotation of the head and the package relative each other. The two markers on the package opening were used as measurement reference during the rescaling. The results of those calculations were written to .txt files, suitable for loading into ABAQUS CAE®.

4.1.2 Drink Sequence Simulation

As only the frames are of interest in the interaction with the lips, the rest of the respective package will be left out in all simulations.

2D Virtual Head Cross Section

The recorded drinking sequences were analysed and in particular the opening of the mouth and the positioning of the lips at the moment just before contact. Based on that analysis the decision was made that it would be sufficient to only draw one head part and use it in all four simulation scenarios. The

first frame used for extraction of coordinates for the markers in the movie corresponding to the scenario 'A38 F' was chosen as a background sketch to draw the contour of the head (shown in Figure 4.4(b)). The origin of the model was chosen to be the marker on the ear. The nasal bridge of the test subject was measured and used as measurement reference for scale calibration.

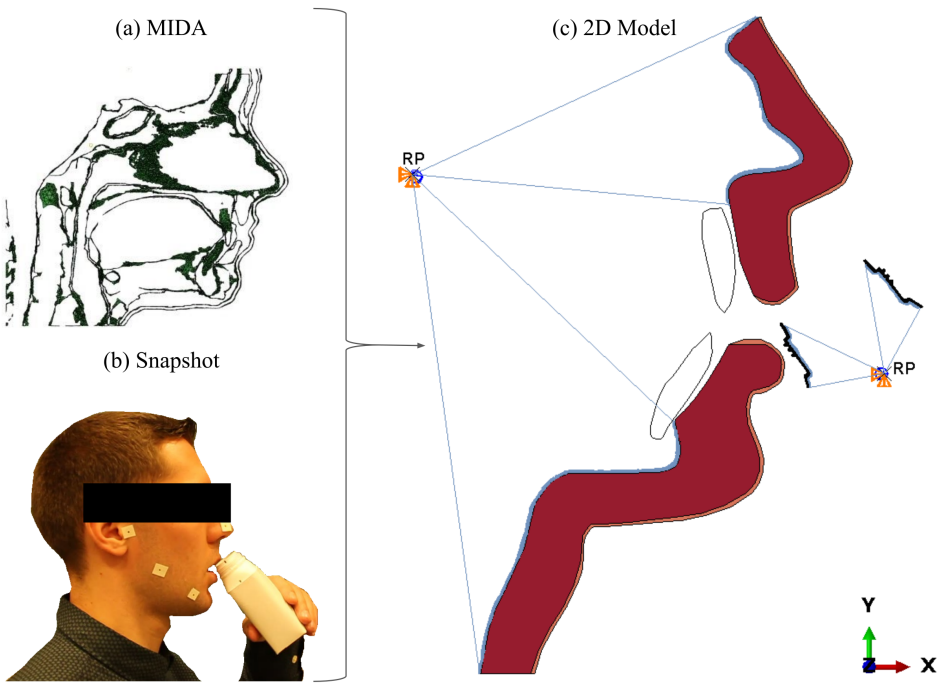

Figure 4.4: a), Overview of tissues from MIDA used as support when sketching internal features for the 2D model. b), Snapshot from 'A38 F' drinking sequence used as contour for the 2D model. c), Model setup for 'A38F' scenario. The blue lines show which edges that were constrained to respective reference point.

When the internal features of the head were drawn and decided (e.g. positioning of teeth, tissue thicknesses, bone placement) a cross-section of some of the *.stl-files from MIDA were used as support. The *.stl-files used are presented in Table 4.1.

The cross section of the *.stl-files can be seen in Figure 4.4(a). The head was drawn as two separate bodies, one comprised of the upper lip and nose and the other one comprised of the lower lip, chin and the neck. This was done by, firstly, drawing the contour of the head using a snapshot from the 'A38 F' movie, secondly, drawing the total thickness of the soft tissue using the cross section of the *.stl-files as support (e.g. the shape and position of the mandibula) and lastly, dividing the soft tissue into a approximately 1 mm thick dermis layer and a bulk layer making up the rest of the thickness (varying between between 10 and 20 mm). These two sections, 'dermis' and

'bulk' were assigned material properties corresponding to L2 Ogden. One upper and one lower tooth modelled as rigid bodies were placed behind the lips.

The inner side of the upper and lower part of the head and the upper and lower teeth were constrained to a reference point at the origin using coupling constraints. The inner side of the lower and upper lip were left unconstrained. The frame (either the A38 or the DC) was positioned and given an initial rotation according to the calculations derived from the motion analysis. The inner sides of the packages were constrained through a coupling constraint to a reference point positioned according to the lower marker on the frame/neck.

Surface-to-surface contact properties were given to the teeth, the lips and the package. Friction between the package and the lips was modelled using penalty friction formulation with a friction coefficient of 1.0 (chosen as a in between value based on the coefficients mentioned in section 2.2) and the contact between the teeth and the lips was modelled as frictionless. The set up of the 'A38 F' model can be seen in Figure 4.4(c). The package necks were meshed using $\approx$ 5000 elements for each neck and the head was meshed using $\approx$ 20000 elements. The elements used were primarily linear quad elements with reduced integration but some linear triangular elements were also used.

Table 4.1: The various surfaces imported into Hypermesh™ to generate the final geometry used in simulations.

Name of the tissue *.stl file	Description
Muscle - Orbicularis Oris	Muscle surrounding the mouth
Mandible	Bone of the lower jaw
Skull	The bone of the skull and upper jaw
Skull Outer Table	Skull bone situated beneath the scalp
Teeth	-
Tongue	-
Epidermis_Dermis	The outer skin layers combined
Adipose Tissue	Fat tissue in general
Subcutaneous Adipose Tissue	Fat tissue beneath the skin
Mucosa	Thin skin layer covering among other the inside of the nose and mouth
Muscle (General)	General collection of facial muscles
Air internal - oral cavity	Cavities where no tissue is to be found

For the scenario 'A38 AE' the lower part of the head and the lower tooth were

moved in order to better resemble the positioning of the lips according to the recorded drinking sequence. The simulations were run using the dynamic implicit solution scheme. The step time used was 4.0 for the 'F' scenarios and 8.0 for the 'AE' scenarios. The step times were chosen in order to minimise kinematic effects. As it was not obvious whether to approximate the simulations as plane stress or plane strain, 'A38 F' were run using plane strain and plain stress assumptions and the results were compared. The decision was made to use plane stress in the following simulations, as the deformations at the contact areas were almost identical and the plane stress simulations were more robust. For the scenario 'DC AE' a force was applied on the upper lip at the beginning of the simulation in order for the upper lip to bend outwards so it could enclose the package frame. This was achieved through a trial and error process, simply by guessing a magnitude and direction of the force. Performed so as to mimic the actual recorded lip placement embracing the DC frame. All four scenarios were run and the run time varied between 45-120 minutes.

3D Partitioned Virtual Head

The 3D domains were obtained by use of the finite element pre-processor Hypermesh™ included in Altair®'s software suite Hyperworks® and subsequent manipulation of the *.stl-files included in the MIDA licence.

Initially all the surface meshes were imported into Hypermesh™. In general the surfaces were initially smoothed by approximation of a new surface mesh to fit the initial domain for a given element size. For some tissues in need of removal of superfluous details a tetrahedral mesh was generated. Thereby subsequent removal of elements automatically retained a watertight bounding surface of the domain (Figure 4.5).

Special treatment of the teeth was needed as teeth from both the upper, and lower jaw were sectioned out as a separate tissue and they were also joined. Thus elements binding the teeth of the upper jaw and the lower jaw together were removed, and the teeth of each jaw were joined with the corresponding bone tissue prior to the smoothing. By performing this union both the upper and lower jaw included teeth, as well as the bones (skull and mandibula = jaw bone, respectively). When sufficiently smooth surface meshes were obtained of the different tissues, continuous geometries were generated from the FE-mesh of the tissues using built in functions in Hypermesh™.

Having generated surface geometries of the epidermis/dermis, the upper, and lower jaw, as well as the tongue and air inside the mouth cavity: the epidermis/dermis layers was used as the outermost bounding surface and then closed of at the throat. Inside of the enclosed volume, a new bounding surface was generated to be used as the subdermis tissue, or bulk tissue. This approximated all volume between the epidermis/dermis down to the bone as

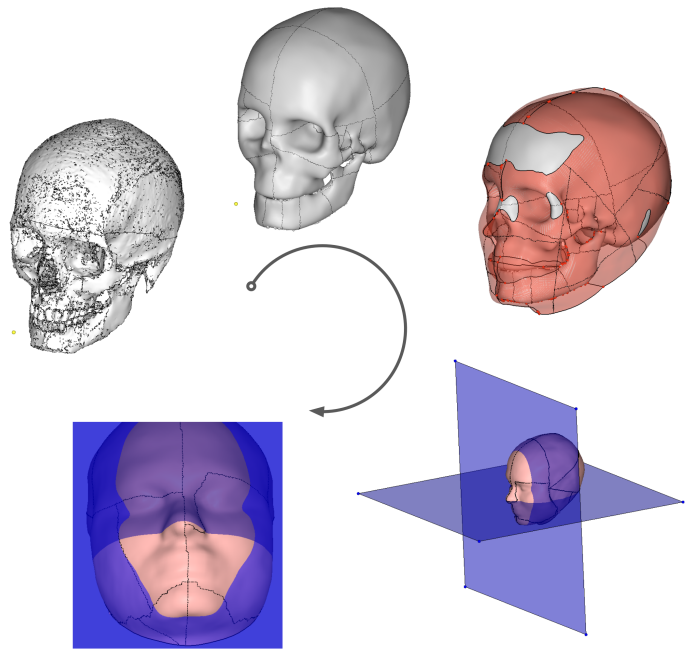

Figure 4.5: The procedure of extracting the 3D mesh. First FE meshes were smoothed and then the subdermis tissue was generated as the remaining volume between the dermis, the bones, the mouth cavity and the tongue. Lastly, the face was sectioned to reduce the computational domain and then meshed using tetrahedral elements.

this intermediate layer. The bounding surface of the subdermis was coincident with the innermost surface of the epidermis/dermis. This enabled the meshes of the subdermis and dermis to be tied to each other easily at their interface. From the subdermis volume the volume of the bones as well as the tongue and the air inside the mouth were removed to create the mouth cavity. This approach created interfaces between the subdermis and the upper and lower jaw, which were used to define tie constraints.

To obtain a realistic thickness of the epidermis/dermis layer, the innermost bounding surface of the epidermis/dermis geometry was used to create a copy of the innermost surface of the epidermis/dermis at an offset specified to be 1.3 mm from the inner surface. These two bounding surfaces were then closed by creation of surfaces, sealing their edges together and thereby creating an enclosed volume. This volume enabled a subsequent generation of a solid mesh. To open up the mouth, sections of the subdermis and dermis surfaces were deleted and the cut surfaces closed to retain the watertight geometries. Thus the shape of the lips was manufactured and not taken from a real scan.

Lastly, all geometries to be used for the virtual head were cut using cutting planes, roughly splitting the head into four domains. These domains were

then meshed: taking care to mesh the tissues being approximated as rigid bodies, i.e. the bones, slightly coarser than the other deformable tissues, i.e. the epidermis/dermis and the subdermis to reduce computational effort. The surface of the epidermis/dermis and the subdermis tissue that were to come into contact with the package frames were meshed using smaller elements and the parts of the tissues further from the mouth were meshed using approximately ten times larger elements. Both the subdermis and epidermis/dermis sections were meshed using 529261 C3D4 tetrahedral elements, with sizes varying between $[0.2, 2.0]$ [mm].

The rigid parts were meshed either using R3D3 for the tria elements or R3D4 for the quad elements. The lower, and upper jaw were meshed using 1126 and 1559 elements respectively using target element sizes ranging from 1 mm to 2mm in the meshing tool in Hypermesh™. For the DC opening device, 28280 elements were generated and for the A38, 75233 elements were generated. For both frames geometry files were supplied by Tetra Pak® and these underwent slight modification to simplify the geometry by removal of superfluous details, such as duplicate surfaces or small features not affecting the soft tissue interaction. For the frames, element sizes ranging between 0.2 mm (frame tip) and 2 mm (parts not coming into contact with the soft tissue) were used.

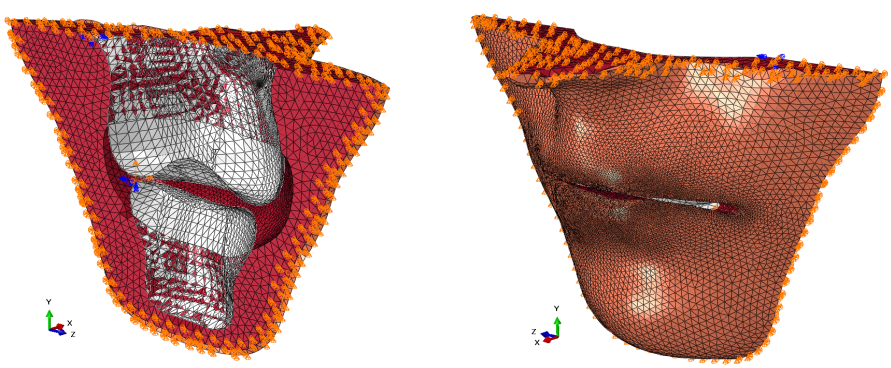

Figure 4.6: The BCs applied on the back and top nodes of the soft tissue domain as well as the lower and upper jaw and their respective BCs.

The assembly was then imported into ABAQUS® 2018 CAE to avoid any compatibility issues arising from the usage of a different version of Hypermesh™. Materials for the dermis and subdermis were the same as in the L2 Ogden configuration. Moreover, the nodes present on the top and at the very back of the soft tissue domain were pinned: locking displacement degrees of freedom only (Figure 4.6). Worth noting is that the nodes bordering the bones had a more lax formulation and were not pinned as this would prohibit the opening motion of the jaws. Remembering that the nodes of the soft tissue simultaneously are included in the tie constraint binding them to the bones, which would lead to conflicting constraints.

The frame was put roughly in the center line of the face and then by using BCs it was brought into contact with the soft tissue. The analysis was specified as a dynamic explicit step of 4 seconds and general contact for all surfaces, including self contact, was defined for the assembly.

The interaction property PKG_TO_SKIN, see Table 4.2, was used in general for the contact but for the inside of the mouth (the purple surface in Figure 4.7) and its contact with the teeth (the blue surface in Figure 4.7) the interaction property INNER_MOUTH_TO_BONE was employed instead.

Table 4.2: Table over the two interaction properties used in 3D simulations.

	PKG_TO_SKIN	INNER_MOUTH_TO_BONE
Normal behaviour	Hard contact, allow separation	Hard contact, allow separation
Tangential behaviour	Penalty friction formulation, $F_c = 1.0$	Frictionless

Furthermore, some surfaces were excluded from the general contact and for some, tie constraints were formulated instead, while for the teeth self contact was neglected, consequently the upper, and lower jaw cannot "feel" one another. In Figure 4.7 the first surface pair of the two tie interfaces is shown as red surfaces where the lower and upper jaw coincide with the subdermis inner surface.

The second of the two tie constraints is displayed in Figure 4.8 where the tie is applied to the surface coloured red which visualises the interface between the dermis and subdermis.

Lastly the step was defined so as to vary the mass of elements to keep the time step close to 5E-05 s during the simulation by use of the *Variable Mass

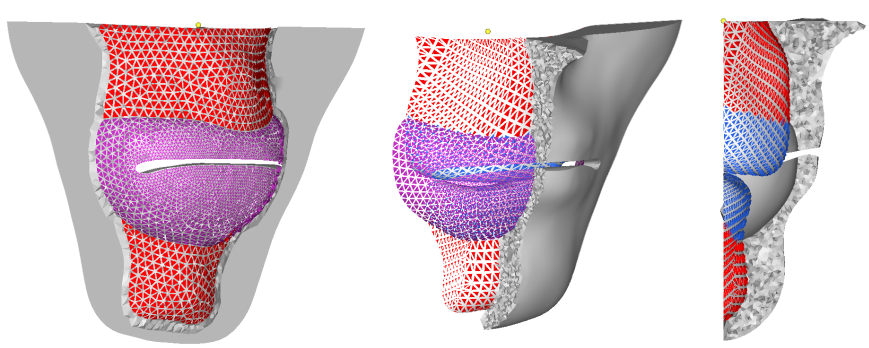

Figure 4.7: The interaction between the subdermis and the teeth. Left: The subdermis (grey) inner surface lining the mouth cavity (purple) and the surface of the subdermis tied to the upper and lower jaw (red). Middle: the same surfaces with an addition of the surface of the teeth (blue). Right: View from the side where the teeth (blue) are seen more clearly as well as the partitioning of the bone where it is tied to the subdermis (red).

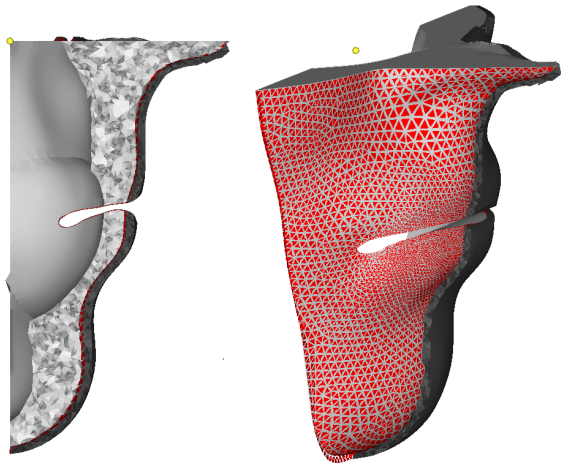

Figure 4.8: The interaction between the subdermis and the dermis. Left: The subdermis (grey) outer surface (red) tied to the dermis (black). Right: View from the front where the dermis have been peeled of from parts of the face revealing the tie between the subdermis and dermis

keyword in ABAQUS® updating the time step every 1000 increment of the simulation to keep the step close to the set value.

To obtain the imprint on the package frame the CPRESS output from ABAQUS® was used, and to obtain the contact area CAREA was output for the frames.

4.2 Results and Analysis

4.2.1 Motion Capture and the 2D Virtual Head Cross Section

Movement Patterns

Before analysing the results of the different scenarios some remarks must be made regarding the obtainment of displacement BCs. Since a camera produces a two-dimensional representation of a three-dimensional setting distances becomes distorted when one tries to convert the pixels in an image to a length scale in SI-units applicable to the whole image. Objects at a different depth than the object used as measurement reference will seem bigger or smaller than they really are. Further problems arise if one applies two markers on an object with the purpose of using those two markers as a measurement reference and that object is rotated placing the two markers at different depths in the image. Then all distances will be distorted to some extent.

Both of these problems were present during the recording of the BCs. The side of the head and the package were at different depths, and the markers

on the packages were not always at the same depth. This combined with the fact that the same head (sketched from the 'A38 F' scenario) was used in all simulations had the consequence that some of the initial positions of the packages and their BCs needed manual editing. The reason for using the same head part in all scenarios was because of the fact that if the packages and movements of the head and package frames were to be varied and compared, any differences in the results originating in structural differences of the head's geometry were to be minimised.

Since 'A38 F' was the case for which the head part was sketched from for all scenarios almost no manual editing was required in order to get realistic movements for the corresponding simulation. Comparing the position of the frame relative to the lips in Figure 4.9 it is seen that for the first four snapshots the result is quite good with one exception: How far the lower lip reaches on the package. In the snapshots from the movie it is clearly seen that the lower lip reaches well below the threads on the frame whilst in the snapshot from the simulation the lower lip barely reaches the lowest thread. In the last snapshot there is no contact in the simulation even though there is in the snapshot from the movie. Both of theses problems are believed to be the result of both the scaling issue mentioned previously and also due to the fact that no muscle activation is present during the simulation.

In order for the initial opening of the mouth to better mimic reality in the 'A38 AE' simulation, it was required that the lower part of the head and the lower tooth were moved in positive X- and Y-direction. The movement of the package required some manual editing in order to obtain a realistic drinking sequence. This editing consisted of running the simulation without contact using a coarse mesh, evaluating the movement, changing the initial position of the package and then running the simulation again until the result was satisfying. When comparing the real life movement with the virtual one in Figure 4.10 it is seen that the results are quite good. However as with the previous case there is a discrepancy regarding the positioning of the lower lip onto the package, once again raising the issue regarding muscle activation.

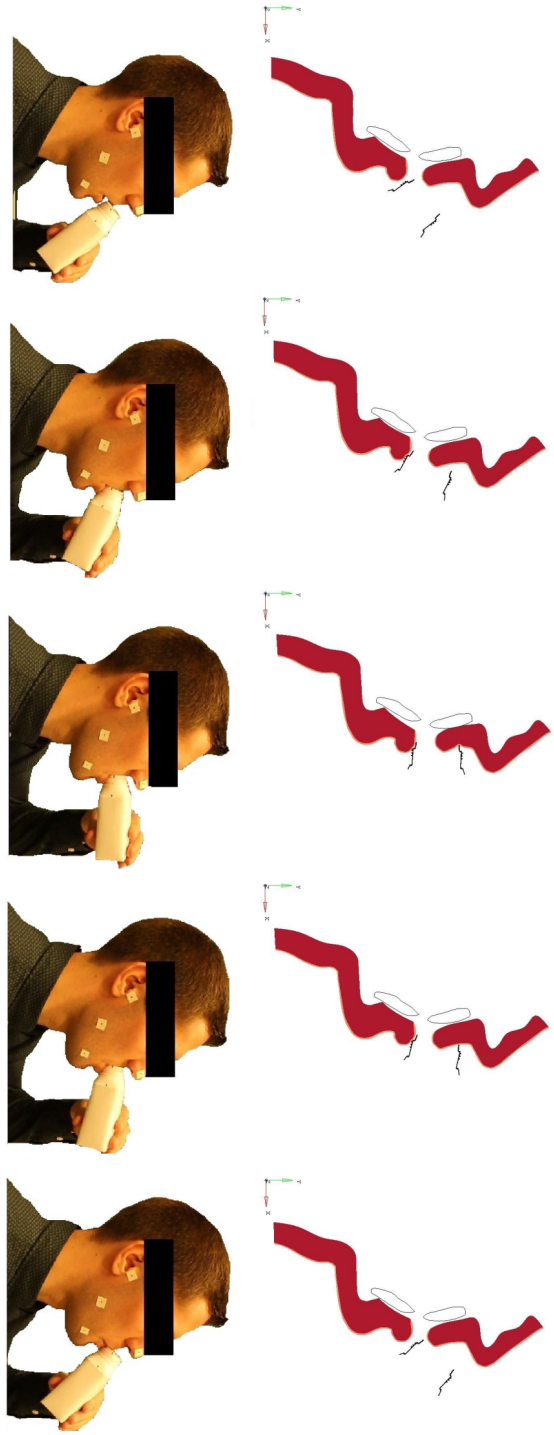

Figure 4.9: Snapshots in time sequence showing both 2D simulation and corresponding recorded drinking sequence for scenario 'A38 F'.

Figure 4.10: Snapshots in time sequence showing both 2D simulation and corresponding recorded drinking sequence for scenario 'A38 AE'.

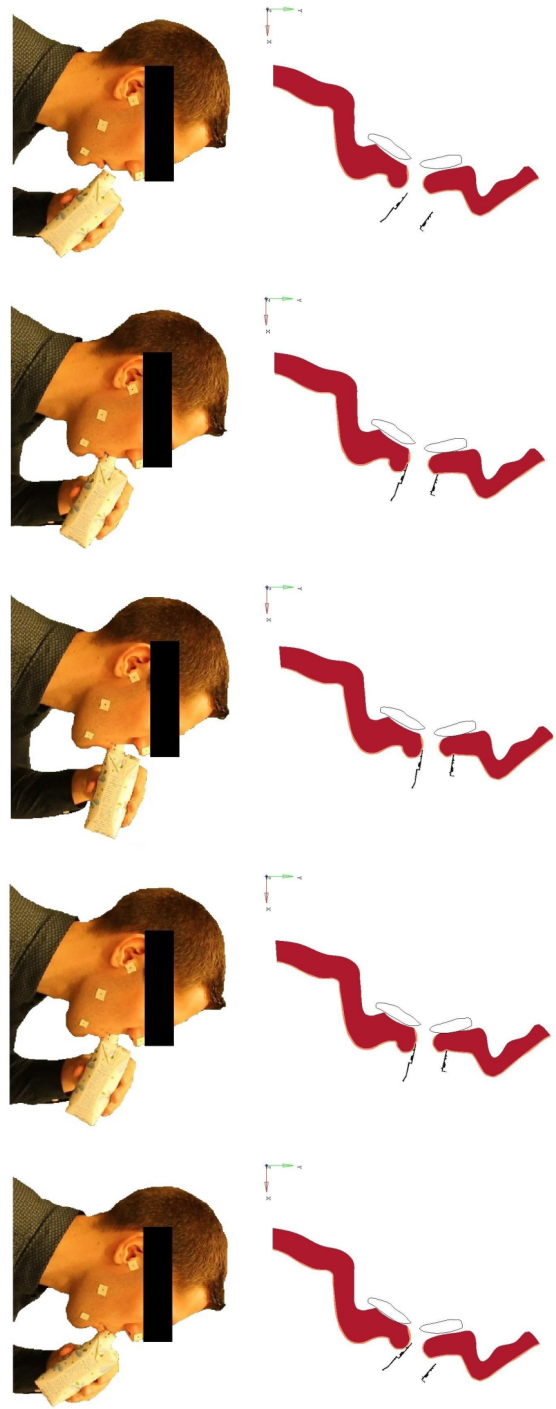

Figure 4.11: Snapshots in time sequence showing both 2D simulation and corresponding recorded drinking sequence for scenario 'DC F'.

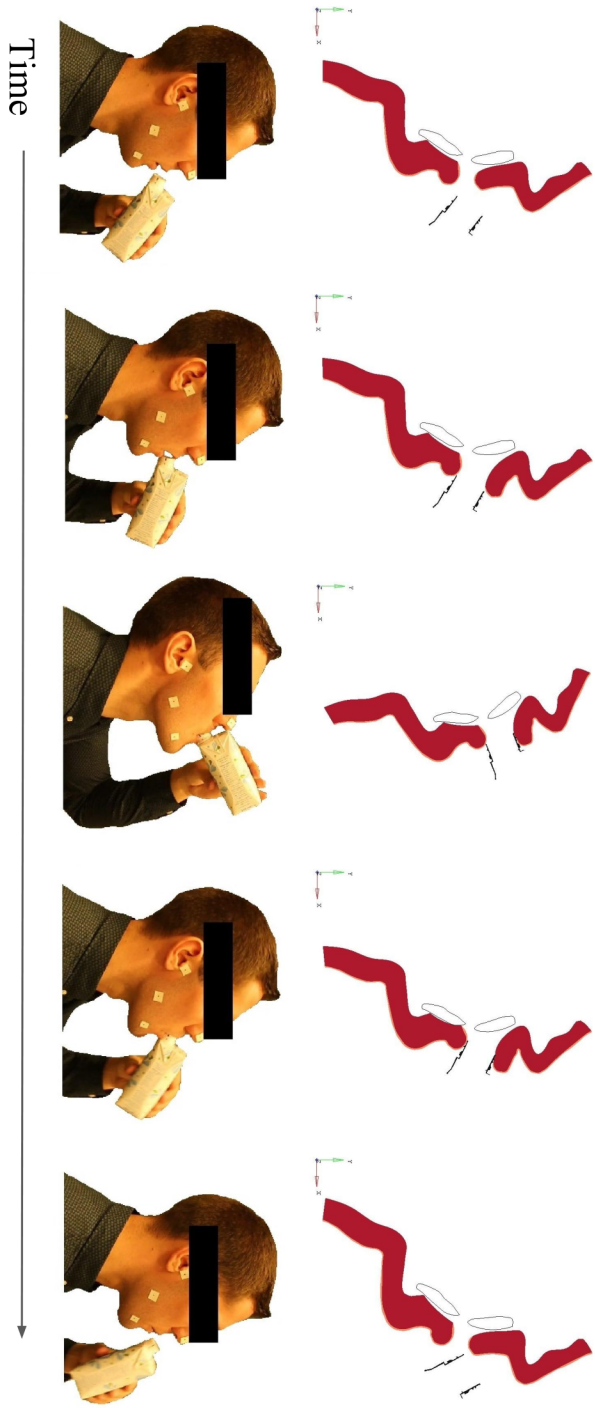

Figure 4.12: Snapshots in time sequence showing both 2D simulation and corresponding recorded drinking sequence for scenario 'DC AE'.

For the case 'DC F' (Figure 4.11) the initial opening of the mouth were similar to that of the case 'A38 F' making the implementation of the movement easier. The only editing required was changing the initial positioning of the package a few millimetres.

Moving on to the simulation with the highest degree of difficulty in terms of making the movement realistic was 'DC AE'. It required manual editing in the amplitude curves associated with the displacement BCs. Furthermore, since the upper lip embraces the package opening, as seen in the second snapshot in Figure 4.12, a pseudo muscle activation was needed in order to obtain a realistic movement.

Getting this pseudo muscle activation correct was a time consuming process as the force applied needed to be within a certain range. If the force was too low the upper lip would not be out of the way for the neck when needed. If the force was too high then the final positioning of the upper lip onto the frame became unrealistic once the force was relaxed. Comparing the snapshots (Figure 4.12) it is seen that the movement in the simulation resembles the reality rather good. However as with all the other cases the positioning of the lower lip fails to be mimicked.

Finally it can be said that it is feasible to reproduce the movements fairly well using simple methods. The question regarding the need of muscle activation is raised in all four cases and is reinforced by the statements mentioned regarding 'suck', 'pull' and 'pour'. Perhaps the most for 'suck' and 'pull' as the 'pour' method is a rather passive way of drinking. Another interesting finding is that the test subject used 'pull' for all four scenarios except the 'DC AE', where he used 'suck'. This indicates that the method of drinking is perhaps not individual, but dependant on the size and shape of the package, the size and shape of the package opening and the amount of content left in the package.

Material Behaviour

The minimum and maximum principal logarithmic strains present in the dermis during the four scenarios are shown in Figure 4.13 and 4.14. When analysing the simulations it was seen that as long as there was any kind of contact present, the maximum stresses and strains in the dermis were found either at the upper or lower point of contact. This was the case for all scenarios except 'DC AE', which had a concentration built up at the nasal base because of the applied force. Looking at Figures 4.13 - 4.14 it is seen that the strains varies between ≈ -0.5 and ≈ 0.25 for the dermis. With these numbers in mind, looking back at Figure 3.20, it is seen that the strains present in the material correspond to the non-linear region of the constitutive relation. This speaks against using an application specific linear elastic model.

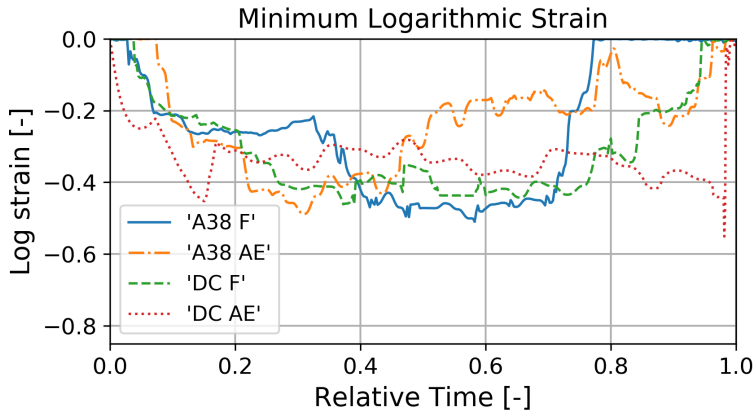

Figure 4.13: The minimum logarithmic strain in the dermis material layer as a function of relative time, for all four scenarios.

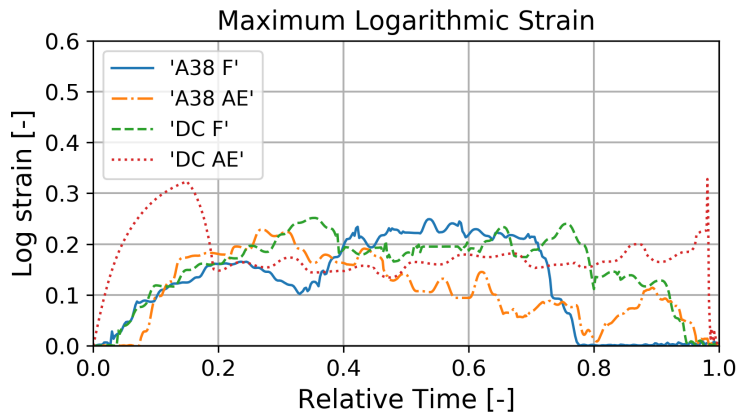

Figure 4.14: The maximum logarithmic strain in the dermis material layer as a function of relative time, for all four scenarios.

The tensile strains lie within realistic magnitudes (recall the mean failure strain of $\approx 50\%$ and that the toe region lies between 0.0 up to ≈ 0.3 logarithmic strain [3]). Due to lack of information regarding compression of skin it is hard to comment upon the compressive strains.

Figure 4.15 shows the maximum von Mises stresses present in the dermis during the simulations. For 'DC AE' there is a peak at the around 0.1 relative time, this is due to the pseudo muscle activation. There is another peak at around 0.98 relative time, this is due to the "snap back" of the upper lip once the package is withdrawn from the mouth. Both of these peaks are neglected when analysing the stresses thus making the maximum stresses in all scenarios lying below ≈ 160 kPa. These graphs are of course affected by the manual editing of the initial positions, BCs etc., but as they lie well below the reported UTS: the stresses are not unrealistic in terms of material response.

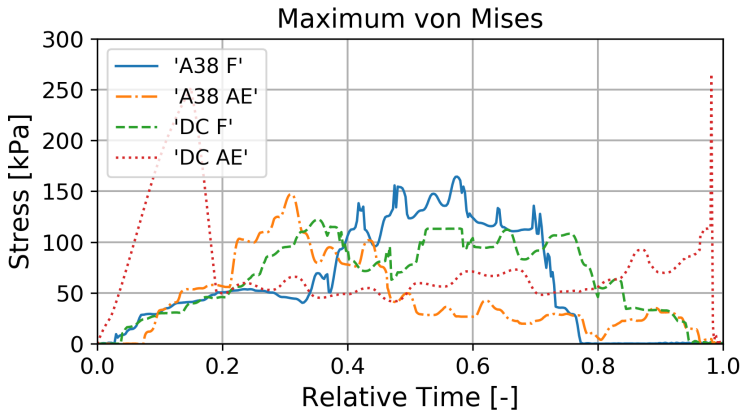

Figure 4.15: The maximum von Mises stress in the dermis material layer as a function of relative time, for all four scenarios.

Furthermore, recalling that the algometry studies mentioned in the literature study stated that a sense of discomfort can appear at contact pressures as low as ≈ 270 kPa the stresses found within the material are considered realistic in terms of application.

Contact Pressures

Figure 4.16 and Figure 4.17 show an average of the two highest contact pressures present between the package and the upper and lower lip respectively.

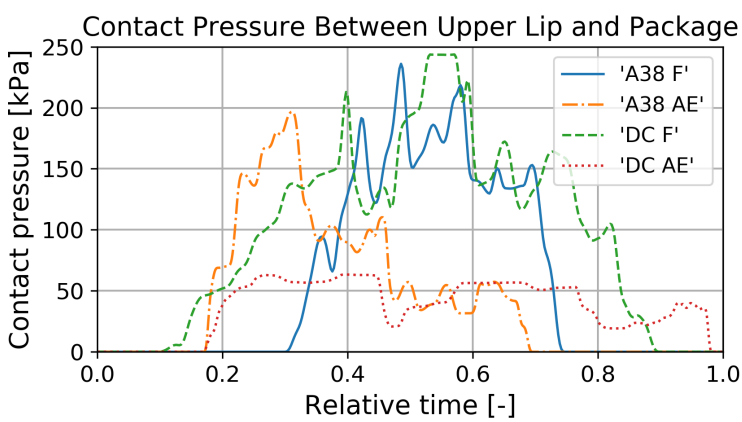

Figure 4.16: Contact pressure between the upper half of the package and the upper lip. The magnitude is calculated as the mean of the two elements exposed to the highest contact pressure in each simulation frame.

Studying the contact pressures between the upper lip and the package (Figure 4.16) it is seen that the curves for the 'F' scenarios peaks around half way in to the drinking sequences. It is also seen that both of those curves are quite symmetric around respective peak. When looking at the 'AE' curves in the same figure one notices that both of those experiences their highest pressure about one third in. Since this is the results from one person drinking one time one should be careful jumping to any conclusions. However, one could imagine that when a person drinks from a package that have just recently been opened (as opposed to a package that is almost empty), said person does so in a more careful manner producing a smoother more protracted curve.

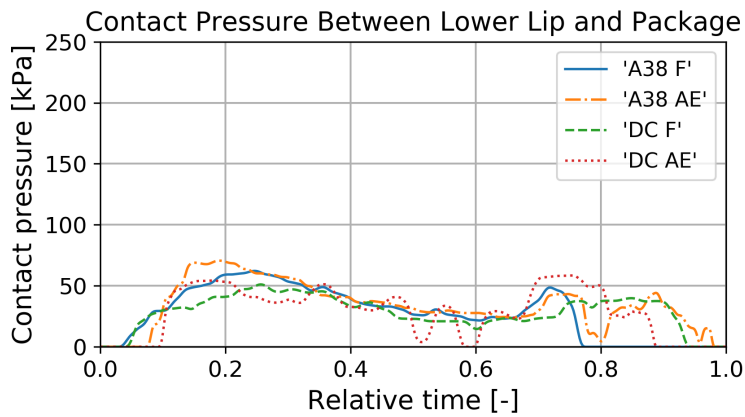

Figure 4.17: Contact pressure between the lower half of the package and the lower lip. The magnitude is calculated as the mean of the two elements exposed to the highest contact pressure in each simulation frame.

When examining the contact pressures present between the lower lip and the package (Figure 4.17) the curves are very similar for all four scenarios. Also, the magnitudes of the pressures are significantly lower than those present at the upper lip. As the package is laid upon the lower lip whilst it is pressed against the upper lip during a drink sequence the differences in magnitudes are perhaps not so surprising. However, these findings raises the question that it is perhaps the upper half of the package opening that should be of most interest when investigating drink feeling experience.

4.2.2 3D Partitioned Virtual Head

Simulation Setup

Beginning by commenting on the 166% difference in the number of elements generated for the two frames: The much higher amount used for the A38 stems from the higher number of threads present compared to the DC. To be able to represent the curvature from the crest down to the root finer elements need to be used and thus the total number of elements increases with more

threads. Furthermore, the A38 is bigger than the DC, which also contributes to the higher amount of elements needed.

It should be noted that the step into 3D is not obvious. The clear advantages of using 3D simulation is that the amount of simplifications forced into the model may be reduced. For the cases of the human head and the drinking action showed in this thesis, the most apparent simplification is the plane stress assumption made for the 2D model (Figure 4.4). One should keep this uncertainty in mind: surely the model may be more completely represented, but simultaneously a much more complex domain must be supplied with BCs for the problem to be accurately defined. An example of this is how to apply the BCs at the borders of the domain. Comparing Figures 4.6 with 4.4, where in 2D one defines the BCs along a line: whereas in 3D one must define how the nodes are allowed to move in the thickness direction as well. Raising questions about how deep the nodes should be pinned and how does the interaction between the different layers affect the boundary conditions and ties in the model?

In retrospect, the mesh of the solid bones should have been refined to reduce the penetrations of the subdermis into the teeth. Nonetheless, as this affected the bulk tissue and not the dermis and the penetrations were small (0.1 mm), it was deemed acceptable. Moreover, the time available to rerun simulations and redefine tie constraints for the bones was too scarce. Furthermore, two problematic C3D4 elements were removed from the soft tissue domain as their volume was close to zero, causing the simulation to exit prematurely. None of the elements were close to the lips and the removal was deemed not to have noticeable impact on the final result.

Keeping to the soft tissue: the choice of defining the geometry of the simulation using continuous surfaces and volumes, in contrast to mesh manipulation, was taken at an early stage. The perks from doing so is that the obtained geometries may be more easily and more accurately cut and remeshed. Stepping away from the initial surface meshes provided in the MIDA license did not come without side affects: As the geometries created out of the surface meshes inevitably became distorted and the dermis layer in particular did not retain the initial variation across the facial region. This was due to the fact that the final dermis was a product of a manufactured surface offset. Thus, the thickness supplied by the MIDA epidermis/dermis surface mesh was lost during the process of creating a more easily modified domain. The main cause of this originated from the authors novice experiences of Hypermesh™ and CAD in general. A more accurate representation of a human face is possible to create out of the MIDA files. The mouth opening in particular caused much trouble as it was to be opened from its initial, closed, state. Editing the surfaces was difficult without affecting much of the geometry of the rest of the domain. Consequently, the final result came out quite crude, though functional. Moreover, one might be fooled by the fact that no vermilion is vis-

ible for the lips to distinguish them from the rest of the face. This originates in the time consuming work of editing the geometry.

Moving on to prescribed conditions in the model, several simplifications have been used. Firstly, from the interaction between the subdermis, i.e. the muscles and subcutaneous fat in the face, and the bones it is not clear that they should be tied to each other. Some speak of a sliding layer enabling some movement of the soft tissue relative the bones, without actually deforming the soft tissue [40]. The ties used between the subdermis and the bones in these simulations strains the subdermis to a high degree when the opening action of the mouth is performed by the motion of the jaws.

Secondly, the BCs prescribed to the back and upper nodes of the soft tissue (Figure 4.6) should contribute to a stiffer behaviour of the facial tissue as the equivalent would be to fasten the facial skin of a person using threads of extremely sticky glue, not allowing the tissue to move and redistribute itself during deformation. The pre-tension of the skin also comes into play when one seeks to define initial conditions of the facial tissue. One might argue then, that since the simulations performed in this work neglect the pre-tension in the tissue, BCs causing higher strains make up for some of the stress otherwise ignored.

Model Behaviour During Consumption

Figure 4.18: A time series showing a mid cut of the face during the drinking action. Below is the DC frame coloured dark grey where contact is present. CAREA is the total area of the frame in contact with the face.

Figure 4.19: A time series showing a mid cut of the face during the drinking action. Below is the A38 frame coloured dark grey where contact is present. CAREA is the total area of the frame in contact with the face.

Comparing the colouring of the frames in Figures 4.18 and 4.19 to what can be expected it seems as if the soft tissue is slightly more rigid than can be expected as the colouring of the frames never reach very close to the root of any of the threads. Nor did the contact spread to a wider area comparable to Figure 3.25(d), instead it seems as if elements in contact with the frame have enforced a slight distance between the frame and nearby tissue. This might have to do with the first order tetrahedral elements used as they are unable to describe bending in a satisfactory manner and provide too stiff a structure if the mesh is not fine enough.

Since the simulation is set up in an displacement controlled fashion there is no limit to what strains may be inflicted upon the soft tissue as the frame has a set trajectory trough space and would literally be able to move mountains. Naturally, one would adapt the package to ones mouth during the drinking action by force feedback through sensory nerves. This is why recorded motion of the face and of the package, as well as some force feedback, is preferable for simulation to acquire more realistic deformations.

Nonetheless, the fidelity of the deformations seen in Figures 4.18 and 4.19 is high. Of course in comparison with the two dimensional simulations the motion of the package and face are directed and not recorded. They are formulated such that the motion is realistic even though it is not real. Sampled motion could, with some more time, be realised with the same means as those used for the 2D simulations. Either with the addition of at least an extra camera tracking the bodies depth-wise, as well as recording the motion of the frame and face in the plane. Or by assuming planar motion of the package frame and making the simplification of only recording jaw movement. By doing so, one still neglect muscle activation by letting the soft tissue adapt to the jaws during the drinking action and thus only adaptation of data from the BCs of the 2D simulations is required.

Contact Pressures

Analysing the magnitude of the contact pressures is not taken to be top priority as the dermis during the simulations is subject to strains outside of its calibrated zone. Instead looking at the shape of the contact areas trends are visible for the DC and for the A38. In Figures 4.18 and 4.19 one may note two things looking at the final time step ($t = 4.0$ s):

- Firstly the indentation of the upper lip is more severe when analysing the A38 if compared to the DC. Keeping in mind that the drinking action is controlled by BCs this is still believed to be a consequence of the larger opening of the A38 frame, as it reaches higher up towards the nose.
- Secondly the area in contact is approximately the same for both the

frames (≈ 42 mm^2 for the DC vs ≈ 43 mm^2) for the A38. Considering the larger geometry of the A38 this should indicate that the contact pressure could be higher on the A38 as is should otherwise come into contact with more skin than the DC.

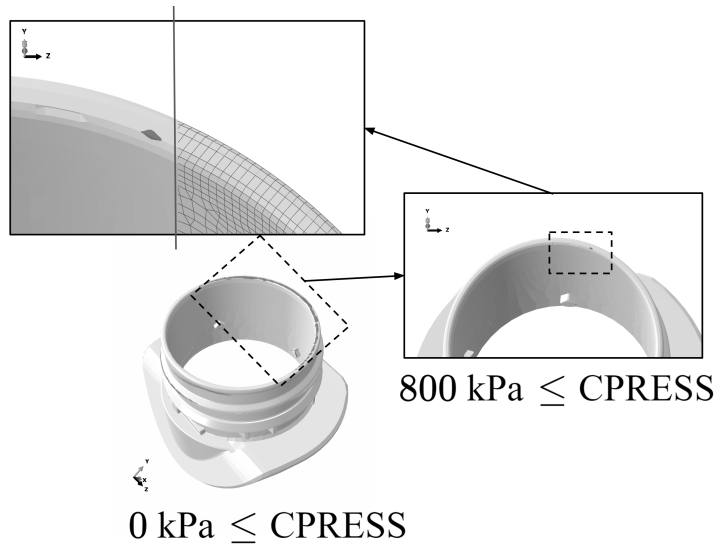

Figure 4.20: For the DC frame. Bottom: showing all areas where contact is present. Right: areas where the contact pressures are higher than 800 kPA. Top: zoom in of the image to the right, showing the element size to be compared with the size of the area in contact.

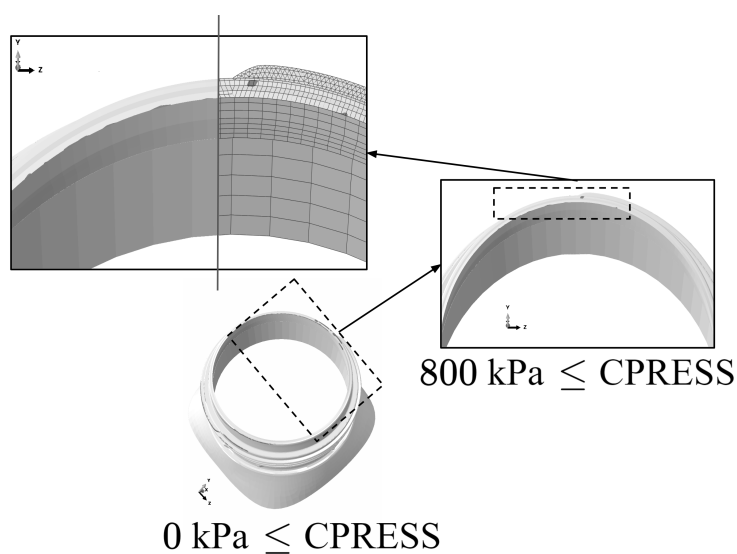

Figure 4.21: For the A38 frame. Bottom: showing all areas where contact is present. Right: areas where the contact pressures are higher than 800 kPA. Top: zoom in of the image to the right, showing the element size to be compared with the sizes of the areas in contact.

This notion is backed by the results showed in Figures 4.20 and 4.21, in which areas of high contact pressures of the DC come down to being a single spot having a contact pressure higher than 800 kPa. In contrast to the A38, which has several spots along the edge hitting the upper lip which demonstrate high contact pressures above 800 kPa. Comparing this to the graphs in Figures 4.17 and 4.16, the trend from the 2D simulations that the contact pressure is highest on the upper lip is kept also when performing similar simulations in 3D.

Returning to Figures 4.20 and 4.21 it is evident that there are more critical areas of the A38, but the results require validation and should be subject to a high mesh dependency as sharp corners always attract stress concentrations. The validation should be used to ascertain whether the contact pressures seen in the simulations are close to pressures present during real consumption and also to investigate the mesh dependency in the model. Thus, both the package opening devices and the face should be included in mesh studies to know whether the results are not just artefacts from inferior meshing. The element sizes are quite large when compared to the size of the areas of high contact and this could have impact on the results (Figures 4.20 and 4.21).

The Drinking Action

In Figure 4.22 the contact of the upper lip, visualised using blue colour, is a direct consequence of the pouring drinking motion modelled (also visible in Figures 4.23 and 4.24)

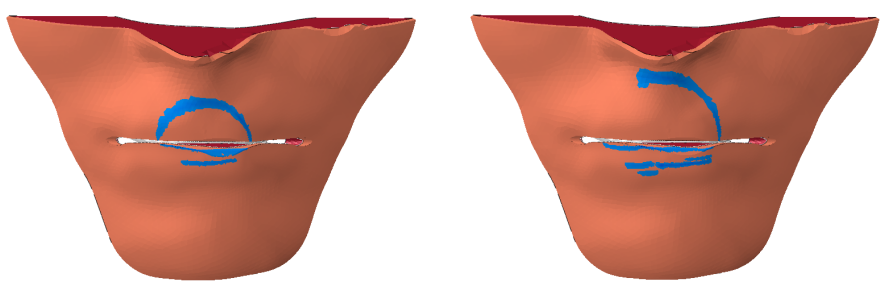

(a) The DC frame.

(b) The A38 frame.

Figure 4.22: The drinking action, where the blue coloured elements in the dermis are in contact with the package frames. This time the contact pressure is plotted on the undeformed mesh. In a) is the imprint from the DC frame at $t = 4.0$ s and in b) is the A38 frame imprint at $t = 4.0$ s for comparison.

For both package frames, the motions of the jaw and the frame trajectory were modelled to be as similar as possible. Despite this, there are differences in the BCs governing both of these motions and in the end the simulations were deemed functional from how they looked. Thus, the bulging of the lips and where the opening device indented the soft tissue were key factors when

reviewing the package motion and the fidelity of the simulation (Figures 4.23 and 4.24).

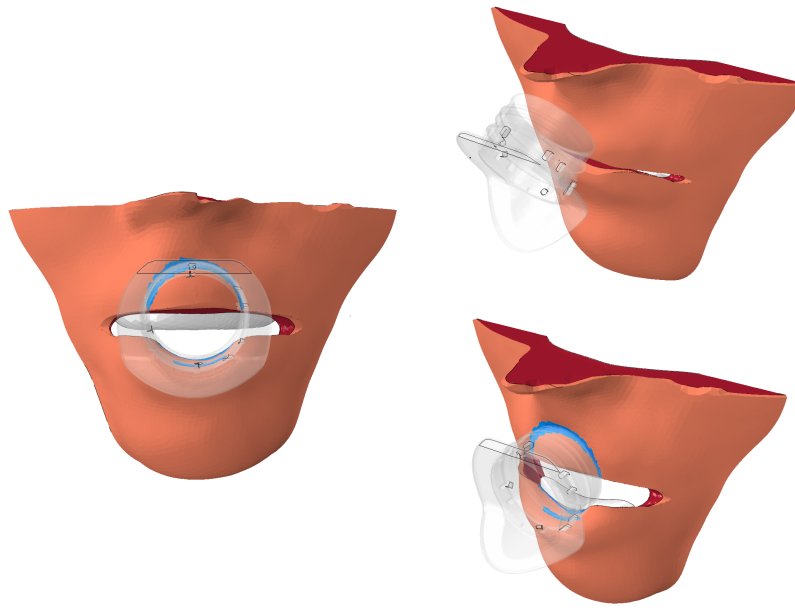

Figure 4.23: The drinking action, where the blue coloured elements in the dermis are in contact with the DC package frame. The frame itself has been made transparent to enhance visibility.

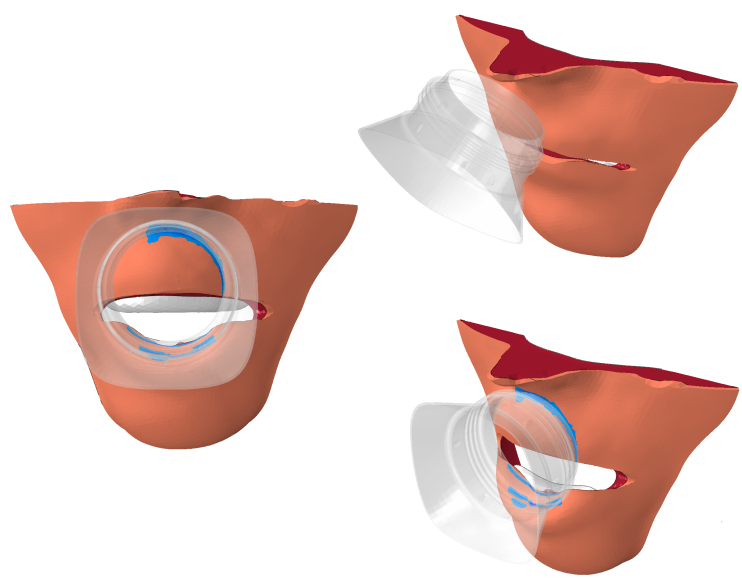

Figure 4.24: The drinking action, where the blue coloured elements in the dermis are in contact with the A38 package frame. The frame itself has been made transparent to enhance visibility.

Material Behaviour

Progressing to the constitutive attributes of the materials chosen it should be noted that with the goal of excluding parts of the domain heavily deformed by the jaw motion in itself, only elements close to where the frame came into contact with the dermis were included when extracting the data shown in Figures 4.25 and 4.26. Starting off, the strain ranges in the dermis is investigated by plotting the maximum and minimum logarithmic strain (Figure 4.25(a) and 4.25(b)). Comparing the DC to the A38, the maximal strains of the A38 are $\approx 30\%$ higher. A similar trend is true also for compression where the minimum strains for the A38 are $\approx 40\%$ lower than the DC minimum strains. It does not seem strange that a frame with a wider opening causes higher strains, as the tissue should deform to a higher degree if stretched by friction.

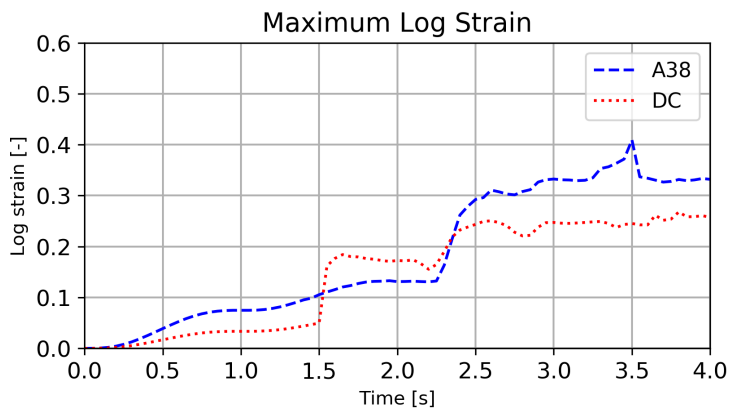

(a)

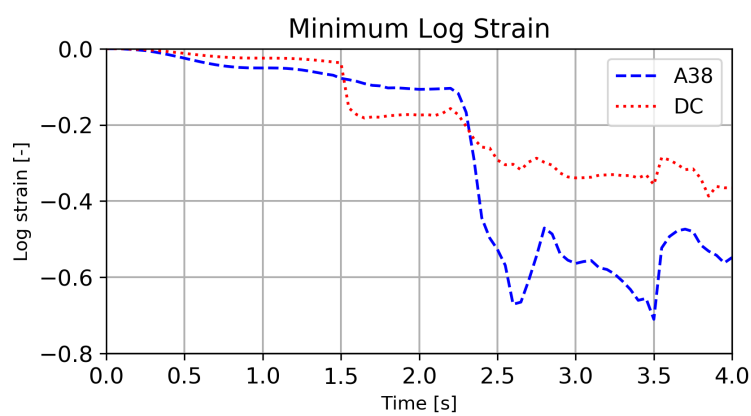

(b)

Figure 4.25: a) The maximum logarithmic strain, and b) the minimum logarithmic strain: in the dermis for the elements close to the mouth, including both frames.

Turning to the maximum von Mises stress (Figure 4.26) the A38 displays

greater stresses, which is to be expected when reviewing the strains which are inflicted by the frame (Figure 4.25(a) and 4.25(b)). Moreover, a stress peak stands out in the A38 graph (at time 3.5 s). It should be due to the frame pushing the tissue to the teeth and thus it is rather a result of the motions in the simulation and not something connected to the frame itself.

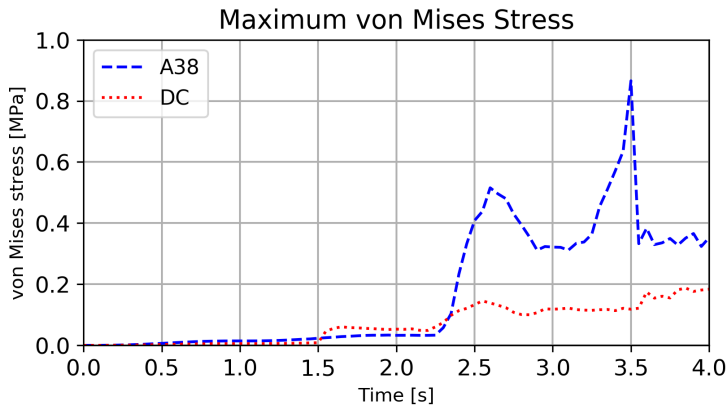

Figure 4.26: The von Mises stress in the dermis for the elements close to the mouth, including both frames.

Analysing the behaviour of the dermis in the graphs in Figures 4.25(b) and 4.25(a): it is subject to high maximum strains if compared to values provided in Table 2.3 (50% engineering strain is equivalent to 41% logarithmic strain). Thus the skin in the simulations might acquire damage during the drinking action, which is totally unfeasible. Considering that both these frames are on the market today and that people do not cut their lips drinking from them. Nonetheless, the maximal von Mises stresses in Figure 4.26 keeps within feasible bounds when considering the algometry studies and the PPT and PPTO values reported in Table 2.4, but this should come from the mild hardening displayed in the material chosen (Figure 3.20). Moreover, comparing the strains in the drinking simulations with those obtained during material calibration (Figure 3.13, p.33) they are considerably higher during the drinking simulation than what the material has been calibrated for.

The origin of the high strains may come from the previously mentioned BCs and the tie constraints formulated for the underlying tissue. Or, they might stem from the incomplete modelling of the structure of the facial tissue, which could allow for areas of excess skin to be unfolded during tension. Perhaps it is even so that facial skin is more extensible, more susceptible to deformation, without acquiring damage, than for instance back or abdomen skin. Especially in the corners of the mouth, during the opening action, high strains developed as the tissue in the corners was stretched open by the motion of the jaws. This is thought to be an artefact of the incomplete knowledge of the structure of the lips, simultaneously living soft tissue is capable of high

deformation with little or no damage. Clearly lack of actual data on the subject makes it hard to tell whether these strains are realistic or a consequence of the simplified soft tissue domain, which contains to creases and no initial strain. An intermediate fix to this could of course be to deform the facial domain prior to contact and then save the deformed face to be used as input into the drinking simulation without transferring the strain state of the domain.

Chapter 5

Discussion

In the beginning of this work we set out to formulate properties of the human skin and how to model them by choosing a hyperelastic strain energy as material model. That was to lay the foundation onto which a drinking simulator could be set up, by having calibrated the material chosen so as to obtain realistic deformations. In this drinking simulator, we then evaluated the concept of performing virtual product testing by letting package opening devices interact with a model of a human face. Both in 2D and in 3D.

The skin model, L2 Ogden, enable pressure sensitivity analysis to be performed and also provides realistic deformations during simulation of human facial tissue. This can be used in studies where any type of contact interaction involving a human face where deformation and strain states are relevant.

Though one must keep in mind that the model is the product of several approximations and that we in this work chose to ignore influence of: age, gender, viscoelastic effects and also the collagen dependency (which provides anisotropy). Moreover, to include the collagen dependency, to the authors' knowledge, one must then sample from each individual. Something, which is not easily done if the model is to be formulated for a statistically relevant number of subjects. Before performing such measurements, one could quantify the error of neglecting the anisotropy for the strain ranges of the application and perhaps refrain from including the collagen dependency.

Lastly the skin model has been developed using data which is in the low- to moderate strain range, and no data from the skin of the lips has been used in calibration. For the calibration the data does come from the facial region of a human so it is close, but still it is part of the lower lip, i.e. just above the chin. Considering the high intra-subject variability, this should have effect on the material parameters obtained through optimisation. In summary this creates a tissue that may only be adapted to different persons by its thickness.

Proceeding to the modelling of a virtual consumer, the motion capture technique has several benefits as it provides displacement controlled simulations with realistic BCs. Additionally the motions can be used to validate the simulation setup material-wise and identify erroneous approximations. That is, we can see and check whether the deformation of the tissue is correct and if the strain state of the material is unrealistic, then there is work to be done in describing the soft tissue correctly. One must still keep in mind that the method of motion capture performed in this thesis has its limitations as the drinking action was assumed to be performed in a plane. As some motion in the depth direction occurred, the accuracy was impaired.

Furthermore, we have simplified many of the complexities of both the geometry of the face (its anatomy) and also the properties of the tissue: There are no muscles present (affecting the stiffness of the facial tissue), gravity was neglected (affecting deformations) and the thickness of the skin is close to constant over the entire domain, which should have impact on deformations. Especially in the lips, as it should be thinner in that region. Lastly the interactions between the various layers are difficult to model correctly as the facial tissue *in vivo* acts like a black box only providing a bulk response. Consequently it is extremely difficult to specify these interactions: which has great impact on the strain in the tissue, as sometimes the tissue is moved rather than deformed.

Nevertheless, the model of a virtual consumer produced is ready to be used for pressure analysis, where one is interested in how the geometry of a given product, e.g. an opening device, interacts with human facial tissue. It is also capable of providing output regarding where contact is initiated, thus it can direct designers to make well informed choices of the shape and size of a product.

5.1 Future work

As is common when working on a project during a finite amount of time there is work left to do, as one during the course of the work acquires new knowledge and ways of improvement, or new tests needed to be performed. This thesis work is no exception. First and foremost improvements are to be made to the existing work.

Starting of with a more accurately built 3D model which fully utilises the tissue thicknesses supplied from the scanned data and which also has a more accurately modelled mouth opening. On top of this a comparison with different element formulations should be made for the three dimensional simulations of the drinking action as C3D4 elements are known to inflict higher stiffness in the model if the mesh density is not sufficiently high.

Moreover, as facial tissue is pre-stressed this should be implemented in the

model. One way would be through usage of inverse FEM as in [15] to map the stress field across the face *in vivo*. Furthermore, as human skin is clearly viscoelastic: this effect should be quantified for the load cases in mind and implemented if the dissipative effects are significant. Further investigation of the frictional coefficient between the human dermis/epidermis and the material of the frames should be performed as this impacts the interaction visibly.

Additionally the model should be improved to include muscular activity, which is present during the drinking action, but to the authors' knowledge has not been quantified. The activation of muscles should cause stiffening of the facial tissue, both from the shortening of muscular fibres and from increased blood flow into the activated area. This should improve the model's stress/strain response during the drinking action, as well as enabling control of facial expressions.

Analysing future prospects, one major concern throughout the execution of this project was the lack of experimental data more relevant to the application. That is, data on human facial tissue and quantitative results on what deformations that would occur in a load case similar to the one present during the drinking action.

Thus, an experiment similar to the one performed by Tran *et al.* [38], where *in vivo* deformation was recorded using MRI, would be very attractive to perform. Making the area of interest the facial region instead. One could then, with crude geometries, obtain deformation data which could then be used in analysis of more complex shapes such as package frames.

Additionally, by using motion capture, the drinking movements for several test subjects could be sampled in order to obtain "typical" load cases. This should be done using different packages, with varying fill degrees. By doing this, it would also be possible to either reinforce or disprove the belief that the main area of interest is the interaction happening at the upper half of the package opening. Also, the data provided from motion capturing could be used in ergonomic studies investigating, for example, neck tilt angles when drinking.

Another interesting way to develop the model would be a study in line with the algometry study performed by Finocchietti *et al.* [13]. It could be of interest, trying to quantify the drinking sensation and when something is considered pleasant in relation to drink feeling. This data could then be used in pressure studies of different designs.

Finally, in contrast of the chosen approach, where existing material tests performed on actual human skin are used: one could use synthetic materials instead. Since the actual lip material has not been obtained and probably would demand subject-to-subject testing and calibration, a synthetic material would allow for a more fast paced work flow. Using panel tests to obtain data

on discomfort levels, which could later be used in calibration of experimental tests using silicone gels [34]. These synthetic materials could then be used in simulations, where a greater variability of geometries and load cases are allowed for. The advantages of using a synthetic material will be the well defined constitutive relations connected to the material and the low variability of the material, as well as the ease at which it may be obtained. Especially as no ethical concerns arise when using synthetic materials, in contrast of performing tests on live subjects. It would also open up the possibility to scan drinking sequences using, for example computed tomography.

Chapter 6

Conclusion

The outcome of this thesis can be summarised as:

- A material model, that was chosen from existing literature, which had its parameters calibrated using inverse FE-modelling adapted from existing literature. This made it suitable to use when performing simulations of the drinking sequence when the tensile strains (true strain) lie in a range of $[0.0, 0.15]$.
- The calibrated material model, implemented in a 2D simulation, was also validated to investigate compressive behaviour and it showed realistic mechanical response in relation to experimental results: Both in respect of contact area, and also in respect of deformation.
- 2D and 3D virtual models replicating the experimental drinking sequence have been developed in which the interaction with package opening devices may be analysed. The models enable output of critical design criteria such as contact pressure and area, as well as a general insight into how a person drink, regarding the motion and placement of the package frame. These models show that package frames may be evaluated, prior to manufacturing, by using a human-like virtual consumer

Bibliography

[1] *Abaqus Analysis User´s Manual (2018), Dassault Systèmes®, SIMULIA Corp., Providence, USA.*

[2] Alessandra Aldieri et al. "Implementation and validation of constitutive relations for human dermis mechanical response." In: *MEDICAL & BIOLOGICAL ENGINEERING & COMPUTING* 56.11 (2018), pp. 2083–2093. ISSN: 01400118.

[3] Aisling Nì Annaidh et al. "Characterization of the anisotropic mechanical properties of excised human skin". In: *Journal of the Mechanical Behavior of Biomedical Materials* 5.1 (2012), pp. 139–148. ISSN: 1751-6161. DOI: https://doi.org/10.1016/j.jmbbm.2011.08.016.

[4] Various Authors. *Skin: Introduction.* 2018. URL: https://histology.leeds.ac.uk/skin/ (visited on 02/04/2019).

[5] D.L. Bader and P. Bowker. "Mechanical characteristics of skin and underlying tissues in vivo." In: *Biomaterials* 4.4 (1983), pp. 305–308. URL: http://ludwig.lub.lu.se/login?url=http://search.ebscohost.com/login.aspx?direct=true&db=inh&AN=2181224&site=eds-live&scope=site.

[6] J.M. Benìtez and F.J. Montáns. "The mechanical behavior of skin: structures and models for the finite element analysis." In: *Computers & Structures* 190 (2017), pp. 75–107.

[7] OpenStax College. *Anatomy and Physiology.* OpenStax CNX. URL: http://cnx.org/contents/14fb4ad7-39a1-4eee-ab6e-3ef2482e3e22@11.1.

[8] Stephen C. Cowin and Stephen B. Doty. *Tissue Mechanics. [electronic resource].* New York, NY : Springer Science+Business Media, LLC, 2007., 2007. ISBN: 9780387368252.

[9] S. Derler and L.-C. Gerhardt. "Tribology of Skin: Review and Analysis of Experimental Results for the Friction Coefficient of Human Skin". In: *Tribology Letters* 45.1 (Jan. 2012), pp. 1–27.

[10] Michael Dunn and Frederick Silver. "Viscoelastic Behavior of Human Connective Tissues: Relative Contribution of Viscous and Elastic Components". In: *Connective tissue research* 12 (Feb. 1983), pp. 59–70. DOI: 10.3109/03008208309005612.

[11] John D. Enderle and Joseph D. Bronzino. *Introduction to biomedical engineering.* Amsterdam ; Boston : Elsevier/Academic Press, cop. 2012, 2012. ISBN: 9780123749796.

[12] S.L. Evans. "On the implementation of a wrinkling, hyperelastic membrane model for skin and other materials." In: *Computer Methods in Biomechanics and Biomedical Engineering* 12.3 (2009), pp. 319–332. ISSN: 10255842.

[13] Sara Finocchietti et al. "Pressure-induced muscle pain and tissue biomechanics: A computational and experimental study." In: *European Journal of Pain* 15 (2011), pp. 36–44. ISSN: 1090-3801.

[14] Cormac Flynn, Andrew Taberner, and Poul Nielsen. "Modeling the Mechanical Response of In Vivo Human Skin Under a Rich Set of Deformations". In: *Annals of Biomedical Engineering* 39.7 (July 2011), pp. 1935–1946. ISSN: 1573-9686. DOI: 10.1007/s10439-011-0292-7.

[15] Cormac Flynn et al. "Simulating the three-dimensional deformation of in vivo facial skin." In: *Journal of the Mechanical Behavior of Biomedical Materials* 28 (2013), pp. 484–494. ISSN: 1751-6161.

[16] Y. C. Fung. *Biomechanics : mechanical properties of living tissues.* New York ; Berlin : Springer-Vlg, cop. 1993, 1993. ISBN: 0387979476.

[17] Paolo U. Giacomoni, Thomas Mammone, and Matthew Teri. "Gender-linked differences in human skin". In: *Journal of Dermatological Science* 55.3 (2009), pp. 144–149. ISSN: 0923-1811. DOI: https://doi.org/10.1016/j.jdermsci.2009.06.001.

[18] R.B. (1) Groves et al. "Quantifying the mechanical properties of human skin to optimise future microneedle device design." In: *Computer Methods in Biomechanics and Biomedical Engineering* 15.1 (2012), pp. 73–82. ISSN: 10255842.

[19] RY Ha et al. "Analysis of facial skin thickness: Defining the relative thickness index." In: *PLASTIC AND RECONSTRUCTIVE SURGERY* 115.6 (2005), pp. 1769–1773. ISSN: 00321052.

[20] F. M. Hendriks and Author(s) F. M. Hendriks. "Mechanical Behaviour of Human Skin in Vivo - A Literature Review". In: *Nat.Lab. Unclassified Report 820. Philips Research Laboratories.* 2001.

[21] Maria Ida Iacono et al. "MIDA: A Multimodal Imaging-Based Detailed Anatomical Model of the Human Head and Neck". In: *PLOS ONE* 10.4 (Apr. 2015), pp. 1–35. DOI: 10.1371/journal.pone.0124126.

[22] Blistex Inc. Visited 2018-12-13. URL: http://www.blistex.com/lip-tips/what-are-lips/.

[23] C. Jacquemoud, K. Bruyere-Garnier, and M. Coret. "Methodology to determine failure characteristics of planar soft tissues using a dynamic tensile test." In: *Journal of Biomechanics* 40.2 (2007), pp. 468–475.

[24] Hamed Joodaki and Matthew B Panzer. "Skin mechanical properties and modeling: A review". In: *Proceedings of the Institution of Mechani-*

cal Engineers, Part H: Journal of Engineering in Medicine 232.4 (2018). PMID: 29506427, pp. 323–343. DOI: 10.1177/0954411918759801.

[25] Hyungmin Kim, Philipp Jürgens, and Mauricio Reyes. "Soft-Tissue Simulation for Cranio-Maxillofacial Surgery: Clinical Needs and Technical Aspects". In: *Patient-Specific Modeling in Tomorrow's Medicine*. Ed. by Amit Gefen. Berlin, Heidelberg: Springer Berlin Heidelberg, 2012, pp. 413–440. ISBN: 978-3-642-24618-0. DOI: 10.1007/8415_2011_105.

[26] Jansen L. and Rottier P. "Some Mechanical proterties of Human Abdominal Skin Measured on Excised Strips". In: *Dermatologica* 117 (1958), pp. 65–83.

[27] V. Luboz, E. Promayon, and Y. Payan. "Linear Elastic Properties of the Facial Soft Tissues Using an Aspiration Device: Towards Patient Specific Characterization." In: *Annals of Biomedical Engineering* 42.11 (2014), pp. 2369–2378.

[28] Rona M. MacKie. *Clinical dermatology.* Oxford core texts. Oxford : Oxford University Press, 2003, 2003. ISBN: 019852580X.

[29] "Mechanical properties of human skin in vivo: a comparative evaluation in 300 men and women." In: *Skin Research & Technology* 20.2 (2014), pp. 127–135. ISSN: 0909752X.

[30] M. (1) Melia et al. "Pressure pain thresholds: Subject factors and the meaning of peak pressures." In: *European Journal of Pain (United Kingdom)* 23.1 (2019), pp. 167–182. ISSN: 15322149.

[31] Lazarov N., Siefert A., and Fressmann D. "The CASIMIR Model for Simulation in Seating Comfort Applications - A status update for LS-DYNA". In: 10^{th} LS-DYNA Conference, Würzburg, Germany. 2015.

[32] Aisling Ní Annaidh et al. "Automated Estimation of Collagen Fibre Dispersion in the Dermis and its Contribution to the Anisotropic Behaviour of Skin". In: *Annals of Biomedical Engineering* 40.8 (Aug. 2012), pp. 1666–1678. ISSN: 1573-9686. DOI: 10.1007/s10439-012-0542-3.

[33] "Original Report: Conditioned Pain Modulation and Pressure Pain Sensitivity in the Adult Danish General Population: The DanFunD Study." In: *Journal of Pain* 18 (2017), pp. 274–284. ISSN: 1526-5900.

[34] N. Ravikumar et al. "A constitutive model for ballistic gelatin at surgical strain rates." In: *Journal of the Mechanical Behavior of Biomedical Materials* 47 (2015), pp. 87–94. ISSN: 18780180.

[35] Niels Saabye Ottosen and Matti Ristinmaa. *The mechanics of constitutive modelling.* Lund : Dept. of Solid Mechanics, University of Lund, Cop. 1996, 1996.

[36] E. Skoda. "On-the-go: The Trend that's Here to Stay". In: *Packaging Europe* (Oct. 2017). Visited 2019-03-18. URL: https://packagingeurope.com/on-the-go-food-convenience-trend/.

[37] C. Then et al. "New methodology for mechanical characterization of human superficial facial tissue anisotropic behaviour in vivo". In: *Journal of the Mechanical Behavior of Biomedical Materials* 71 (2017), pp. 68–

79. ISSN: 1751-6161. DOI: https://doi.org/10.1016/j.jmbbm.2017.02.022.

[38] H.V. (1) Tran et al. "In vivo characterization of the mechanical properties of human skin derived from MRI and indentation techniques." In: *Computer Methods in Biomechanics and Biomedical Engineering* 10.6 (2007), pp. 401–407. ISSN: 10255842.

[39] Eric P. Widmaier et al. *Vander's human physiology : the mechanisms of body function.* New York : McGraw-Hill, 2014, 2014. ISBN: 125908082X.

[40] T. Wu, A. Hung, and K. Mithraratne. "Generating Facial Expressions Using an Anatomically Accurate Biomechanical Model." In: *IEEE Transactions on Visualization and Computer Graphics* 20.11 (2014), pp. 1519–1529.

Appendix A

Complementing Theory

Notation

In this thesis the notation stated below will be employed when using tensor algebra and mathematics: Let $\bar{e}_i$ denote the base vector, and let: $\bar{a} = \sum_i a_i \bar{e}_i$, denote a first order tensor, $\bar{\bar{A}} = \sum_{i,j} A_{ij} \bar{e}_i \bar{e}_j$, a second order tensor, and $\bar{\bar{\mathbb{A}}} = \sum_{i,j,k,l} A_{ijkl} \bar{e}_i \bar{e}_j \bar{e}_k \bar{e}_l$ a fourth order tensor respectively.

$$\bar{a} \cdot \bar{b} = \sum_i a_i b_i \qquad \bar{a} \otimes \bar{b} = \sum_{i,j} a_i b_j \bar{e}_i \bar{e}_j$$

$$\bar{\bar{A}} : \bar{\bar{B}} = \sum_{i,j} A_{ij} B_{ij} \qquad \bar{\bar{A}} \cdot \bar{\bar{B}} = \sum_{i,j,k} A_{ik} B_{kj} \bar{e}_i \bar{e}_j$$

$$\bar{\bar{A}} \cdot \bar{b} = \sum_{i,j} A_{ij} b_j \bar{e}_i \qquad \bar{\bar{\mathbb{A}}} : \bar{\bar{B}} = \sum_{i,j,k,l} A_{ijkl} B_{kl} \bar{e}_i \bar{e}_j.$$

Strain Energy Parameters

Starting off by introducing the deformation gradient going from an undeformed configuration to the deformed through

$$\bar{\bar{F}} \equiv \frac{\partial \bar{x}}{\partial \bar{X}^T}, \tag{A.1}$$

For material coordinates $\bar{X}$ and spatial coordinates $\bar{x}$. From the deformation gradient the Jacobian, or total volume ratio, is defined by taking the determinant of eq. (A.1) providing

$$J \equiv det(\bar{\bar{F}}) \tag{A.2}$$

From the volume ratio the elastic volume ratio in [1] is defined as the ratio between the thermal volume ratio and the total volume ratio

$$J^{el} = \frac{J}{J^{th}}; \text{Isothermal setting} \Rightarrow J^{th} \equiv 1. \tag{A.3}$$

Now define the modified left Cauchy Green strain tensor as

$$\tilde{\bar{B}} \equiv J^{-1/3}\bar{\bar{F}} \cdot J^{-1/3}\bar{\bar{F}}^T = \tilde{\bar{F}} \cdot \tilde{\bar{F}}^T. \tag{A.4}$$

From eq. (A.4) the deviatoric stretches may be defined as

$$\hat{\lambda}_i \equiv \sqrt{eig(\tilde{\bar{B}})}, \quad \text{for } i = 1, 2, 3, \tag{A.5}$$

and the first deviatoric strain invariant may also be defined from eq. (A.4) according to

$$\hat{I}_1 \equiv trace(\tilde{\bar{B}}^T \cdot \tilde{\bar{B}}) = \sum_{i=1}^{3} \hat{\lambda}_i^2 \tag{A.6}$$

Furthermore in eq. (2.6) the quantity $\langle \hat{E}_i \rangle$ is defined according to

$$\langle \hat{E}_i \rangle = \langle \kappa(\hat{I}_1 - 3) + (1 - 3\kappa)(\hat{I}_{4(ii)}) - 1 \rangle, \quad \text{no sum on i,} \tag{A.7}$$

where the Macauley bracket, $\langle \cdot \rangle$, is defined in accordance with [1] as

$$\langle a \rangle = \frac{1}{2}\left(|a| + a\right). \tag{A.8}$$

$\hat{I}_{4(ii)}$ in eq. (A.7) is defined by using the fibre directions $\bar{A}_i$ in the GOH strain energy (eq. (2.6)) through the equation

$$\hat{I}_{4(ii)} \equiv trace(\bar{A}_i \otimes \bar{A}_i \cdot \tilde{\bar{F}}^T \cdot \tilde{\bar{F}}), \quad \text{no sum on } i \tag{A.9}$$